Check for updates

View Article Online
View Journal

Dalton Transactions
An international journal of inorganic chemistry

Accepted Manuscript

This article can be cited before page numbers have been issued, to do this please use: K. T. O'Donoghue, D. Geddes, T. Wilkinson, M. C. Stennett, B. Kim, D. Iuga, M. Hayes and B. Walkley, *Dalton Trans.*, 2026, DOI: 10.1039/D6DT00775A.

This is an Accepted Manuscript, which has been through the Royal Society of Chemistry peer review process and has been accepted for publication.

Accepted Manuscripts are published online shortly after acceptance, before technical editing, formatting and proof reading. Using this free service, authors can make their results available to the community, in citable form, before we publish the edited article. We will replace this Accepted Manuscript with the edited and formatted Advance Article as soon as it is available.

You can find more information about Accepted Manuscripts in the Information for Authors.

Please note that technical editing may introduce minor changes to the text and/or graphics, which may alter content. The journal's standard Terms & Conditions and the Ethical guidelines still apply. In no event shall the Royal Society of Chemistry be held responsible for any errors or omissions in this Accepted Manuscript or any consequences arising from the use of any information it contains.

ROYAL SOCIETY OF CHEMISTRY

rsc.li/dalton

View Article Online
DOI: 10.1039/D6DT00775A

High-field multinuclear MAS NMR and synchrotron XANES reveal the influence of strontium salt chemistry on geopolymer nanostructure

Kyle T. O'Donoghue[1], Daniel A. Geddes[1], Tom J. Wilkinson[1], Martin C. Stennett[1], Byoungkwan Kim[1], Dinu Iuga[2], Martin Hayes[3], Brant Walkley[1]*

[1]*School of Chemical, Materials and Biological Engineering, The University of Sheffield, Sheffield, UK*

[2]*Department of Physics, University of Warwick, Coventry, UK*

[3]*United Kingdom National Nuclear Laboratory, Warrington, UK*

Corresponding author: Email: b.walkley@sheffield.ac.uk

Open Access Article. Published on 17 June 2026. Downloaded on 6/17/2026 11:56:12 PM.
This article is licensed under a Creative Commons Attribution 3.0 Unported Licence.

Abstract

This study investigates the influence of strontium (Sr) salt chemistry ($Sr(OH)_2{\cdot}8H_2O$, $SrCO_3$, $Sr(NO_3)_2$, and $SrSO_4$) on the nanostructural evolution of potassium silicate-activated geopolymers. High-field multinuclear (^{27}Al, ^{29}Si, ^{39}K, and ^{87}Sr) MAS NMR, synchrotron XANES, EPMA, XRD, and FTIR showed that while the primary binding phase in all samples is a disordered, highly cross-linked K-A-S-H gel, the Sr immobilisation mechanism is governed by salt solubility. Soluble nitrate and hydroxide salts release Sr^{2+} ions that are chemically incorporated into the K-A-S-H gel framework in brewsterite-type pseudo-zeolitic environments. In contrast, insoluble carbonate and sulfate salts act primarily as physical fillers, and are encapsulated as discrete particles within the geopolymer matrix, though sulfate additionally reacts to form secondary crystalline kalistrontite ($K_2Sr(SO_4)_2$). Sr^{2+} adsorption on metakaolin surfaces is found to inhibit early-stage Al dissolution, resulting in a Si-rich K-A-S-H gel that transitions to an Al-rich K-A-S-H gel over 28 days. These results provide new insight into the mechanisms of immobilisation of Sr in geopolymers, and highlight their potential as wasteforms for long-term management of ^{90}Sr radioactive waste.

Dalton Transactions Accepted Manuscript

View Article Online
DOI: 10.1039/D6DT00775A

Open Access Article. Published on 17 June 2026. Downloaded on 6/17/2026 11:56:12 PM.
This article is licensed under a Creative Commons Attribution 3.0 Unported Licence.

Dalton Transactions Accepted Manuscript

1 Introduction

Nuclear power generation produces a wide range of radioactive waste streams that require appropriate conditioning prior to secure disposal. Among these wastes is strontium-90 (^{90}Sr), a fission product commonly present in reactor cooling water and in complex legacy waste inventories at facilities such as Sellafield and Fukushima Daiichi. Ensuring the safe, long-term disposal of ^{90}Sr is a global priority as efforts to develop deep geological disposal facilities (GDFs) and other disposal scenarios progress [1]. Developing a suitable wasteform capable of providing a robust engineered barrier for ^{90}Sr is key to achieving this.

Cementation offers a low-cost, low-temperature method for conditioning wastes containing ^{90}Sr [2-4]. Because ^{90}Sr in aqueous waste streams is frequently extracted using granular ion-exchange materials, cement-based encapsulation is particularly compatible with this waste type. Portland cement (PC) has traditionally been used for this purpose and is known to bind Sr through chemisorption onto the calcium silicate hydrate (C-S-H) gel phases. The substitution of Ca by ^{90}Sr within PC hydrate phases, especially C-S-H, has also been reported [2, 5].

Much of the ^{90}Sr retention in PC arises from reversible ion-exchange interactions with hydrated or partially hydrated phases in the hardened cement matrix [5]. This limits the extent of true chemical immobilisation, leaving a significant proportion of Sr physically trapped rather than chemically incorporated. Additionally, the high water content of hydrated PC raises concerns regarding radiolytic stability [6]. The substantial CO_2 emissions associated with PC production (accounting for roughly 8% of global anthropogenic CO_2 output) represent another growing concern within the nuclear sector in recent years, particularly regarding long-term sustainability [7, 8]. These issues highlight the need for alternative cementitious systems that can provide sustainable, high-performance immobilisation of ^{90}Sr-bearing wastes.

Geopolymers are promising alternatives to PC-based encapsulants. Their disordered, highly cross-linked aluminosilicate gel network contains cation-binding sites capable of incorporating species such as Sr^{2+} through ion-exchange processes [9, 10]. Geopolymers also exhibit excellent radiolytic stability [11] and possess favourable chemical, mechanical, and thermal characteristics, driving significant interest in their use for radioactive waste immobilisation.

Sodium and potassium are the alkali metals most commonly used in geopolymer synthesis, producing aluminosilicate hydrate gel networks collectively referred to as (N,K)-A-S-H. The nanostructure of these gels is often described as pseudo-zeolitic: while short-range ordering resembles that of zeolites (on the scale of a few Å) [12, 13], the long-range structure is highly disordered and X-ray amorphous. As in zeolites,

View Article Online
DOI: 10.1039/D6DT00775A

Open Access Article. Published on 17 June 2026. Downloaded on 6/17/2026 11:56:12 PM.
This article is licensed under a Creative Commons Attribution 3.0 Unported Licence.

Dalton Transactions Accepted Manuscript

Si and Al occupy tetrahedral coordination environments, with Si typically present in Q^4(mAl) environments and Al most commonly present in Q^4(4Si) coordination. The negative charge introduced by each AlO_4 tetrahedron is balanced by alkali cations [14].

Although previous studies have examined interactions between sodium-activated geopolymers and Sr-bearing wastes, potassium-activated systems have demonstrated superior flow behaviour and rheological properties compared with sodium-based formulations [15-17]. Previous work on potassium-based geopolymers incorporating various strontium salts showed that the anion associated with the strontium salts ($Sr(OH)_2{\cdot}8H_2O$, $SrCO_3$, $Sr(NO_3)_2$, and $SrSO_4$) strongly affected geopolymer reaction mechanisms and kinetics in the fresh geopolymer paste [18], and was controlled in particular by salt solubility. However, the radionuclide incorporation processes which control long-term performance of these materials remain unclear. In particular, there has been little investigation of the influence of the anion associated with salts of strontium on the Sr incorporation mechanism and nanostructural evolution in potassium silicate-based geopolymers in the hardened wasteform.

Solid-state magic angle spinning nuclear magnetic resonance (MAS NMR) spectroscopy investigations of ^{27}Al, ^{29}Si, in geopolymers [19-22] and synthetic N-A-S-H [23] gels have provided significant information about the coordination states of Al and the connectivity of Si in these materials. Further to this, solid state MAS NMR experiments probing ^{23}Na nuclei have revealed new insight into the charge-balancing role of Na, as well as the incorporation of Sr and Ca, in these materials [22]. However, MAS NMR spectra of quadrupolar nuclei such as ^{39}K and ^{87}Sr are much more challenging to measure, particularly in materials with an amorphous nanostructure, and require high magnetic fields not typically available in the laboratory. As such few studies have reported ^{39}K MAS NMR data for geopolymers [24, 25], and to the best of our knowledge none have reported ^{87}Sr MAS NMR data for geopolymers. Previous work, however, has reported ^{87}Sr MAS NMR data obtained at 21.1 T for $SrCO_3$ [26, 27] and $SrSO_4$ [26] and ^{87}Sr MAS NMR data obtained at 7.187 T for $Sr(NO_3)_2$ [28]. ^{87}Sr MAS NMR spectra of inorganic materials such as geopolymers are strongly affected by quadrupolar interactions, with chemical shift distributions contributing insignificantly to the spectral lineshape [29].

This study examines how different strontium salts influence the reaction mechanisms, K-A-S-H gel nanostructural development, and secondary reaction product formation, in potassium silicate-activated geopolymers. The chemical environments introduced by $Sr(OH)_2{\cdot}8H_2O$, $SrCO_3$, $Sr(NO_3)_2$, and $SrSO_4$ simulate the conditions encountered when Sr-bearing waste streams (e.g reactor cooling water, radioactive sludges, slurries, or spent ion-exchange materials) are potentially immobilised within a

View Article Online
DOI: 10.1039/D6DT00775A

Open Access Article. Published on 17 June 2026. Downloaded on 6/17/2026 11:56:12 PM.
This article is licensed under a Creative Commons Attribution 3.0 Unported Licence.

geopolymer matrix. Fourier transform infrared spectroscopy (FTIR), X-ray diffraction, solid-state magic angle spinning nuclear magnetic resonance (MAS NMR) spectroscopy probing ^{27}Al, ^{29}Si, ^{39}K, and ^{87}Sr, synchrotron X-ray absorption near-edge structure (XANES) analysis, and electron probe microanalysis (EPMA) imaging, are used to characterise nanostructural changes induced by the Sr salts, and their influence on Sr incorporation mechanisms. Collectively, the results provide valuable new insight into the nanostructural evolution and Sr incorporation mechanisms in potassium silicate-activated geopolymers, and highlight the suitability of these materials for long-term immobilisation of ^{90}Sr-containing radioactive wastes.

Dalton Transactions Accepted Manuscript

View Article Online
DOI: 10.1039/D6DT00775A

Open Access Article. Published on 17 June 2026. Downloaded on 6/17/2026 11:56:12 PM.
This article is licensed under a Creative Commons Attribution 3.0 Unported Licence.

Dalton Transactions Accepted Manuscript

2 Experimental methods

2.1 Sample preparation

Geopolymers were produced by reaction of metakaolin (MetaMax, BASF, UK, chemical composition provided in Table 1, D_{50} = 4.49 µm) with a solution of potassium silicate. The activating solution was made by reacting potassium hydroxide (AnalaR 99wt.%), deionized water and a potassium silicate solution (PQ-KS, 51.6% potassium silicate, with a solution modulus of SiO_2/K_2O of 2.2, with the balance water, PQ-UK).

Table 1: MetaMax metakaolin chemical composition (wt.%) as determined by X-ray fluorescence analysis (LOI: loss on ignition at 1000 °C).

SiO_2	Al_2O_3	K_2O	Na_2O	MgO	CaO	TiO_2	Fe_2O_3	Other	LOI
52.54	44.54	0.20	0.15	<0.05	<0.05	1.3	0.4	0.2	0.63

Strontium hydroxide octahydrate ($Sr(OH)_2·8H_2O$) (Acros Organics, 98%), strontium carbonate ($SrCO_3$) (Sigma Aldrich, >99.9%), strontium nitrate ($Sr(NO_3)_2$) (Alfa Aeser, 98%) or strontium sulphate ($SrSO_4$) (Alfa Aeser, Reagent Grade) was added to the samples to achieve a constant Sr/Al molar ratio in the final geopolymer binder (Table 2). The H_2O/K_2O ratio for the samples containing $Sr(OH)_2·8H_2O$ take into account the water of crystallisation.

Table 2: Chemical composition (molar basis), water/solids ratio (w/s; mass basis) of the reaction mixtures.

Sample	Anion	Sr/Al	Si/Al	K/Al	H_2O/K_2O	w/s
KGP	-	-	1.5	1.0	11	0.55
OH_1	OH^-	0.025	1.5	1.0	11	0.55
OH_2	OH^-	0.050	1.5	1.0	11	0.55
OH_3	OH^-	0.075	1.5	1.0	11	0.54
OH_5	OH^-	0.125	1.5	1.0	11	0.54
CO_3_1	CO_3^{2-}	0.025	1.5	1.0	11	0.56
CO_3_2	CO_3^{2-}	0.050	1.5	1.0	11	0.57

View Article Online
DOI: 10.1039/D6DT00775A

CO_3_3	CO_3^{2-}	0.075	1.5	1.0	11	0.58
NO_3_1	NO_3^-	0.025	1.5	1.0	11	0.56
NO_3_2	NO_3^-	0.050	1.5	1.0	11	0.58
NO_3_3	NO_3^-	0.075	1.5	1.0	11	0.59
NO_3_5	NO_3^-	0.125	1.5	1.0	11	0.62
SO_4_1	SO_4^{2-}	0.025	1.5	1.0	11	0.56
SO_4_2	SO_4^{2-}	0.050	1.5	1.0	11	0.57
SO_4_3	SO_4^{2-}	0.075	1.5	1.0	11	0.57
SO_4_5	SO_4^{2-}	0.125	1.5	1.0	11	0.60

The activating solution was mixed with metakaolin powder and Sr salt with a high-shear mixer at 1300 rpm for 10 minutes, and the geopolymer paste was then cast in sealed containers and cured for 3 and 28 days at 20°C ± 2°C. After curing samples were immersed in isopropanol to halt the alkali-activation reaction through the removal of loosely bound water. All characterisation was carried out on samples from the same batch.

2.2 Characterisation of the geopolymer samples

2.2.1 X-ray diffraction

X-ray diffraction (XRD) data were obtained across a 2θ range of 5°-70° using a Panalytical X'Pert³ Powder X-ray diffractometer with Cu Kα radiation (1.54 Å), a nickel filter, a step size of 0.020° and a count time of 1 s/ step. Diffracted background intensity at low angles was reduced using an anti-scatter blade, an incident beam divergence of 1.0 mm and a 2.5 ° Soller slit in the diffracted beam were used. Phase identification was performed using the ICDD PDF4+ 2015 database and Diffrac.EVA V4.1 software.

2.2.2 Fourier transform infrared spectroscopy

FTIR spectroscopy data were acquired using a Perkin Elmer Frontier Mid FT-IR spectrometer equipped with a deuterated triglycine sulfate (DTGS) detector and KBr beam splitter optical system, scanning 16 times at a resolution of 4 cm^{-1}. Data were acquired for pellets comprising 200 mg KBr with 2 mg of sample.

Open Access Article. Published on 17 June 2026. Downloaded on 6/17/2026 11:56:12 PM.
This article is licensed under a Creative Commons Attribution 3.0 Unported Licence.

Dalton Transactions Accepted Manuscript

View Article Online
DOI: 10.1039/D6DT00775A

2.2.3 Solid state nuclear magnetic resonance spectroscopy

Solid-state single pulse ^{29}Si and ^{27}Al magic angle spinning (MAS) nuclear magnetic resonance (NMR) spectra were acquired on a Bruker Avance III HD 500 spectrometer at 11.7 T (B_0) using a 4.0 mm dual resonance CP/MAS probe, yielding a Larmor frequency of 99.35 MHz for ^{29}Si and 130.32 MHz for ^{27}Al. A measured 60 s relaxation delay, a 5.5 µs non-selective (π/2) excitation pulse, a total of 512 scans and spinning at 12.5 kHz were used to obtain the ^{29}Si MAS NMR spectra. ^{27}Al MAS NMR spectra were acquired using a 1.7 µs non-selective (π/2) excitation pulse, a measured 10 s relaxation delay, a total of 128 scans and spinning at 12.5 kHz. The same instrument was used to perform the ^{29}Si cross-polarisation (CP) MAS NMR experiments, with the parameters differing only through an initial ^{1}H non-selective (π/2) pulse width of 2.5 µs, a recycle delay of 1.25 s and Hartmann-Hahn contact periods of 2.0 ms. A nominal ^{1}H decoupling field strength of 80 kHz was employed during acquisition and 5120 scans were collected per experiment. The spectra were referenced against pure tetramethylsilane (TMS) at δ_{iso} = 0 ppm for ^{29}Si and 1.1 M solution $Al(NO_3)_3$ at δ_{iso} = 0 ppm for ^{27}Al. The deconvolution of the ^{29}Si MAS and ^{1}H–^{29}Si CP MAS NMR spectra was performed using Gaussian peak profiles. For both of the spectral deconvolutions of each resonance, the isotropic chemical shift (δ_{iso}) and peak full width at half maximum (FWHM) were maintained. Peak intensities were required to be consistent with the structural constraints described by the thermodynamics of a statistical distribution of Si and Al sites within a Q^4 aluminosilicate network for (N,K)–A–S–H gel products [30].

High-field solid state ^{39}K MAS NMR data were acquired at 20.0 T (ν_0 = 39.67 MHz) using a Bruker Avance Neo 850 spectrometer with a Bruker 4.0 mm HX MAS probe which enabled a spinning rate up to 14 kHz. Pulse calibration and chemical shift referencing for all ^{39}K data were achieved using $KCl_{(s)}$ (δ_{iso} = 47.8 ppm) as a secondary reference to the IUPAC primary reference of 0.1M $KCl_{(aq)}$ (δ_{iso} = 0 ppm) [31]. A 'non-selective' π/2 pulse of 12 µs was measured allowing for a 'selective' 4 µs π/2 to be implemented. Spectra were acquired using a double frequency sweep to saturate the central transition followed by a Hahn echo pulse sequence (DFS - p/2 - t - p - acquire) using a measured relaxation delay of 0.1 s and acquiring a total of 480,000 scans per spectra. High-field solid state ^{87}Sr MAS NMR data were acquired at 20.0 T with a Larmor frequency of 36.843 MHz, using a Bruker Avance Neo 850 spectrometer with a Bruker 4.0 mm HX MAS probe, a rotor synchronised double frequency sweep echo pulse, a measured 0.1 s relaxation delay, spinning at 12.5 kHz, and a total of 839,680 scans. ^{87}Sr spectra were referenced against $SrTiO_3$ (δ_{iso} = 63.4 ppm) [27].

Open Access Article. Published on 17 June 2026. Downloaded on 6/17/2026 11:56:12 PM.
This article is licensed under a Creative Commons Attribution 3.0 Unported Licence.

Dalton Transactions Accepted Manuscript

View Article Online
DOI: 10.1039/D6DT00775A

2.2.4 X-ray absorption spectroscopy

XAS data were acquired on the bending magnet beamline B18 at Diamond Light Source, Harwell, UK. Beamline B18 utilises a Pt collimating mirror, a fixed-exit double crystal Si(111) monochromator and a double toroidal focussing mirror. Sr K-edge XAS data were acquired on B18 in transmission mode using finely ground powder specimens dispersed in polyethylene glycol to achieve a thickness of two absorption lengths. Incident and transmitted beam intensities were measured using ionization chambers, filled with mixtures of He and Ar or N_2, operated in a stable region of their I/V curve. Yttrium foil was measured to provide an absolute energy calibration; the first inflection point (in the first derivative) was defined to be 17133 eV. The yttrium foil was measured periodically to ensure that there was no energy drift over the course of the experiment. Data reduction and analysis was performed using the Athena software [32].

2.2.5 Electron probe microanalysis

Electron probe microanalysis (EPMA) was performed using a Jeol 8350F Plus Hyperprobe equipped with energy dispersive X-ray (EDX) and a wavelength dispersive X-ray (4 channel) system. The samples were analysed using beam conditions of an acceleration voltage of 10KV and a probe current of 10nA with a peak coating time of 40 seconds and a measurement of two background (upper and lower) positions for 20 seconds. The intensities of the characteristic x-rays generated by the elements of interest were measured according to their wavelengths by differing crystals, as follows: TAP for Si and Al, PETL for Sr, PETH for Ti and K.

Open Access Article. Published on 17 June 2026. Downloaded on 6/17/2026 11:56:12 PM.
This article is licensed under a Creative Commons Attribution 3.0 Unported Licence.

Dalton Transactions Accepted Manuscript

View Article Online
DOI: 10.1039/D6DT00775A

Open Access Article. Published on 17 June 2026. Downloaded on 6/17/2026 11:56:12 PM.
This article is licensed under a Creative Commons Attribution 3.0 Unported Licence.

Dalton Transactions Accepted Manuscript

3 Results and discussion

3.1 Effect of addition of strontium hydroxide octahydrate to geopolymers

3.1.1 Fourier transform infrared spectroscopy

FTIR data for the geopolymers incorporating $Sr(OH)_2 \cdot 8H_2O$ and cured for 3 and 28 days are shown in Figure S1, Supporting Information, and reveal key vibrational bands that provide insight into their chemical structure and reaction. A dominant band at approximately 1000 cm⁻¹ corresponds to asymmetric stretching of Si-O-T bonds (T = Si or Al) within the aluminosilicate network of the K-A-S-H gel [33]. A shoulder at approximately 1050–1100 cm⁻¹ indicates the presence of unreacted metakaolin, which has a characteristic band at 1060 cm⁻¹ [34]. Additional features include a band at 860 cm⁻¹ related to bridging oxygen in AlO_4 and SiO_4 groups [35], a low-intensity band at 585 cm⁻¹ associated with ring structures of TO_4 units [36], and a small peak at 700 cm⁻¹ is linked to pseudo-lattice vibrations in aluminosilicate rings [22]. A low intensity band at 1420 cm⁻¹ is attributed to asymmetric stretching vibrations of CO_3^{2-} anions in $SrCO_3$ [37], due to reaction of atmospheric CO_2 with excess $Sr^{2+}_{(aq)}$ [38].

Comparing the FTIR data for samples with different Sr/Al ratios shows minimal spectral changes, though the shoulder indicating unreacted metakaolin is more intense in the Sr-containing sample (KGP). This suggests enhanced dissolution due to the alkaline and hydrated nature of $Sr(OH)_2 \cdot 8H_2O$, which raises the solution pH and improves particle wetting. However, previous observations using isothermal calorimetry indicate that this increased dissolution does not enhance gel formation, as higher Sr/Al ratios reduce the total heat released, likely delaying reaction kinetics [18]. The characteristic Si-O-T band does not shift with Sr addition, implying limited structural incorporation of Sr [22, 25]. After 28 days, FTIR spectra show most bands remain unchanged from day 3, confirming early-stage reaction products shape the final structure. The main differences are a shift in the band due to asymmetric stretching vibrations of CO_3^{2-} anions in $SrCO_3$ (1420 to 1480 cm⁻¹) and decreased intensity of the shoulder on the main Si-O-T band due to unreacted metakaolin, indicating continued reaction but no new bond formation.

3.1.2 X-ray diffraction

The X-ray diffraction data for the geopolymer samples containing $Sr(OH)_2 \cdot 8H_2O$ and cured for 3 and 28 days are shown in Figure S2, Supporting Information. The XRD data for each samples cured at 3 and 28 days exhibit a broad feature between 22° 2θ and 35° 2θ, arising from diffuse scattering and consistent

View Article Online
DOI: 10.1039/D6DT00775A

Open Access Article. Published on 17 June 2026. Downloaded on 6/17/2026 11:56:12 PM.
This article is licensed under a Creative Commons Attribution 3.0 Unported Licence.

Dalton Transactions Accepted Manuscript

with the presence of a K-A-S-H gel [39], as well as reflections due to anatase (TiO_2, Powder Diffraction file (PDF) # 01-084-1286) which is present as an impurity in the metakaolin used. The presence of strontium hydroxide octahydrate ($Sr(OH)_2 \cdot 8H_2O$, PDF # 00-027-1438) in samples OH_3 and OH_5 is expected due to the low solubility of the salt [40], although these diffraction peaks are not present in the spectra for samples OH_1 and OH_2. This could be due to the concentration being too small in the samples as, potentially, a greater percentage of the mass of the salt has dissolved into the activating solution resulting in a lower mass percentage of solid salt within the sample. The diffraction spectrum for the OH_2 sample shows that there is strontianite ($SrCO_3$, PDF # 00-005-0418) present. This is most likely due to the carbonation of the geopolymer during exposure to air, forming $SrCO_3$ crystals.

3.1.3 Solid state nuclear magnetic resonance spectroscopy

3.1.3.1 ^{29}Si MAS and ^{1}H-^{29}Si CP MAS NMR

The ^{1}H-^{29}Si CP MAS NMR and ^{29}Si MAS NMR data for the OH_5 and KGP samples cured for 3 and 28 days are shown in Figure 3.

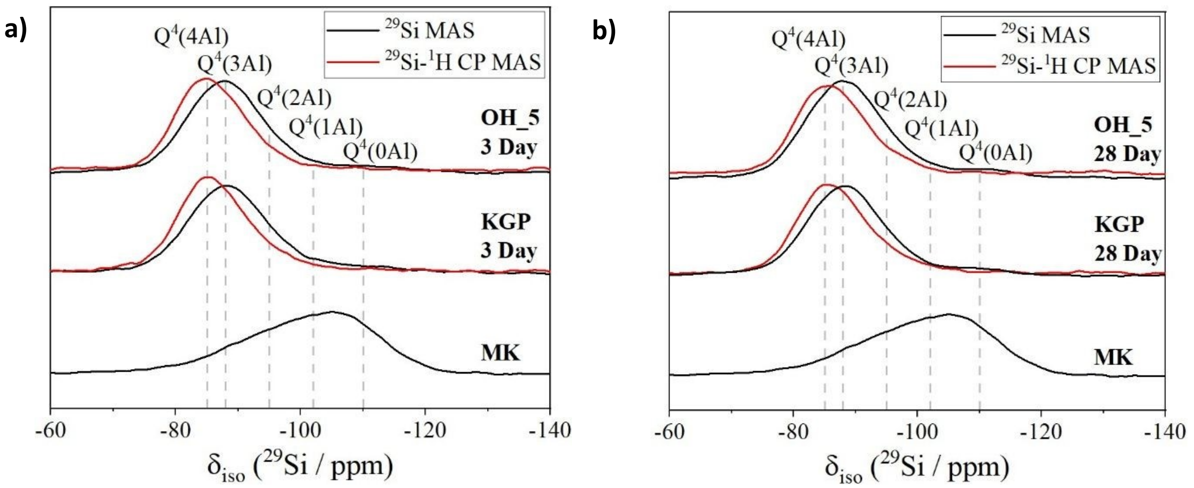

Figure 1: a) ^{1}H-^{29}Si CP MAS (shown in red, B_0 = 11.7 T, ν_R = 12.5 kHz and Hartmann-Hahn contact period t = 2.0 ms) and b) ^{29}Si MAS (shown in black, B_0 = 11.7 T, ν_R = 12.5 kHz) NMR data for geopolymers cured for 3 and 28 days with and without $Sr(OH)_2 \cdot 8H_2O$, and metakaolin.

View Article Online
DOI: 10.1039/D6DT00775A

Open Access Article. Published on 17 June 2026. Downloaded on 6/17/2026 11:56:12 PM.
This article is licensed under a Creative Commons Attribution 3.0 Unported Licence.

Dalton Transactions Accepted Manuscript

The ^1H-^{29}Si CP MAS NMR data for each geopolymer exhibits a broad resonance centred at δ_{iso} = -85.0 ppm and spanning from δ_{iso} = -75 to -100 ppm, with a consistent lineshape for all samples. Si sites in the hydrated K-A-S-H gel can be resolved from those in unreacted metakaolin by comparison of the ^1H-^{29}Si CP MAS NMR data with the ^{29}Si MAS NMR data. The maximum intensity at δ_{iso} = -84.0 ppm in the ^1H-^{29}Si CP MAS NMR spectra of the geopolymer gels, therefore, indicates that the K-A-S-H gel comprises primarily Q^4(4Al) and Q^4(3Al) silicon environments [22, 25, 41, 42]. The data observed here are similar to those seen in previous work, suggesting that the K-A-S-H gel comprises distribution of Q^4(*m*Al) Si sites, where $1 \leq m \leq 4$.

Deconvolution and quantification of the ^1H-^{29}Si CP MAS and ^{29}Si MAS NMR data identifies Q^4(4Al), Q^4(3Al), Q^4(2Al), and Q^4(1Al) sites within an Al-rich (Si/Al ≤ 1.2), fully polymerised K-A-S-H gel [20, 30]. Engelhardt's formula [43] (equation 1) can be used to calculate the molar Si/Al ratio of the K-A-S-H gel by assuming that there are negligible Al-O-Al bonds present (valid in geopolymers with Si/Al > 1 [44]), where , $I_{AQ^4(\mathrm{mAl})}$ represents the normalised relative integral areas of each Q^4(*m*Al) site within the K-A-S-H gel. The relative integral areas and Si/Al for each sample are shown in Table S1, Supporting Information.

$$\frac{\mathrm{Si}}{\mathrm{Al}} = \frac{\sum_{m=1}^{4} I_{AQ^4(m\mathrm{Al})}}{\sum_{m=1}^{4} 0.25 \times m \times I_{AQ^4(m\mathrm{Al})}} \qquad \text{Equation 1}$$

The KGP sample exhibits a slight increase in Si/Al ratio from 1.32 at 3 days to 1.34 at 28 days, supporting the assumption that Al-O-Al bonds are negligible in this system. The OH_5 sample shows consistently higher Si/Al ratios than KGP at both time points. This suggests that the high Sr/Al ratio slightly reduces the gel's ability to incorporate cations, a finding that differs from previous work which reported lower Si/Al ratios in Sr-containing systems [22].

The elevated Si/Al ratio in the OH_5 sample is attributed to the preferential dissolution of Al_2O_3 over SiO_2 in metakaolin [19]. Previous work has shown that Sr adsorbs onto the metakaolin surface during reaction, inhibiting the dissolution of Al_2O_3 relative to SiO_2 and increasing the gel Si/Al ratio. The slight decrease in this ratio from day 3 to day 28 in OH_5 implies that metakaolin continues to dissolve over time, consistent with the FTIR data presented above.

View Article Online
DOI: 10.1039/D6DT00775A

3.1.3.2 ^{27}Al MAS NMR

^{27}Al MAS NMR data for all samples (Figure 2) exhibit a broad resonance centred at δ_{obs} = 60.3 ppm and spanning from δ_{obs} = 70 to 50 ppm, which indicates Al within a tetrahedral (q^4) site in a K-A-S-H type gel [19, 44], promoted by the significant excess of alkali cations able to balance the negative charge due to Al^{3+} in tetrahedral coordination. The preference of Al to exist within the q^4(4Si) coordination is due to the energetic penalty associated with Al-O-Al bonding [30, 45]. A low intensity resonance observed at δ_{obs} = 5 ppm is attributed to the presence of octahedral Al sites (AlO_6) within the samples [46]. The intensity of this peak is negligible when compared to that of the tetrahedral Al peak, and suggests that the majority of the Al within the metakaolin has reacted as the octahedral peak corresponds exclusively to the Al found within the unreacted metakaolin [19]. This is supported by the findings of both the ^{29}Si MAS and ^{1}H-^{29}Si CP MAS NMR data which display the preferential dissolution of Al during the dissolution phase of the reaction. No differences in either resonance are observed when comparing samples with and without Sr.

Open Access Article. Published on 17 June 2026. Downloaded on 6/17/2026 11:56:12 PM.
This article is licensed under a Creative Commons Attribution 3.0 Unported Licence.

Dalton Transactions Accepted Manuscript

View Article Online
DOI: 10.1039/D6DT00775A

Open Access Article. Published on 17 June 2026. Downloaded on 6/17/2026 11:56:12 PM.
This article is licensed under a Creative Commons Attribution 3.0 Unported Licence.

Dalton Transactions Accepted Manuscript

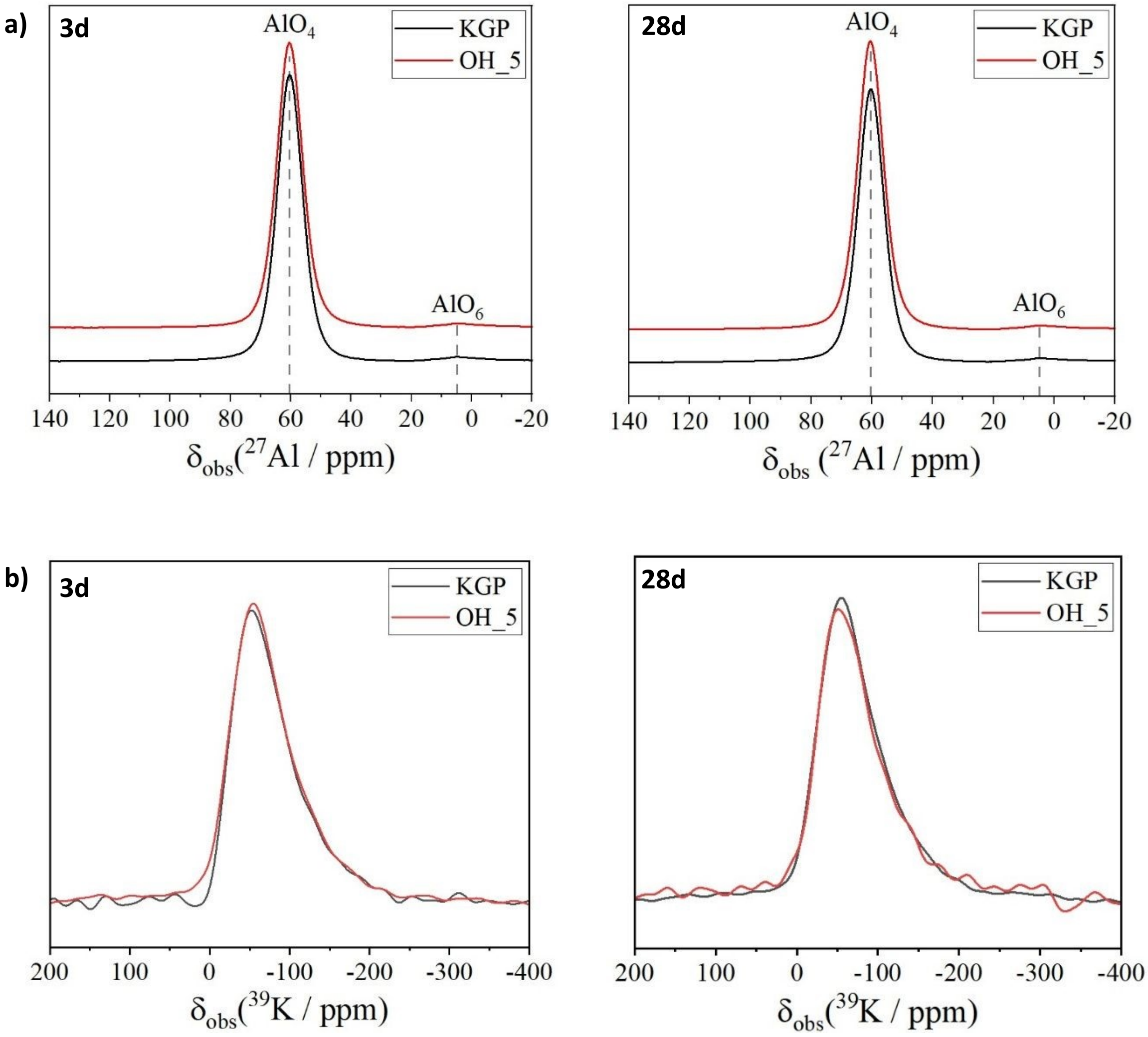

Figure 2: a) ^{27}Al (B_0 = 11.7 T, ν_R = 12.5 kHz) and b) ^{39}K MAS NMR data (B_0 = 20.0 T, ν_R = 12.5 kHz) for each geopolymer cured for 3 and 28d with and without $Sr(OH)_2{\cdot}8H_2O$, as marked.

3.1.3.3 ^{39}K MAS NMR

The ^{39}K MAS NMR data (Figure 2) for the geopolymer samples formulated with and without $Sr(OH)_2.8H_2O$ each exhibit a broad resonance spanning from δ = 0 ppm to -220 ppm, centred at δ = -50 ppm for geopolymers incorporating $Sr(OH)_2.8H_2O$ and δ = -55 ppm for the KGP samples. The resonance exhibits a broad asymmetric lineshape which is characteristic of a quadrupolar nucleus in a disordered material. This resonance is attributed to charge-balancing extra-framework K^+ ions within the K-A-S-H-type gel [24, 25], and the line shape of the data for all samples is comparable, suggesting little change to the chemical environments experienced by the K atoms within the sample. The difference in chemical shift observed in

View Article Online
DOI: 10.1039/D6DT00775A

Open Access Article. Published on 17 June 2026. Downloaded on 6/17/2026 11:56:12 PM.
This article is licensed under a Creative Commons Attribution 3.0 Unported Licence.

Dalton Transactions Accepted Manuscript

the data here is consistent with the shielding of K^+ cations due to the presence of Sr^{2+} in the charge balancing sites within close proximity to K, consistent with incorporation of Sr^{2+} into the K-A-S-H gel to form a K-(Sr)-A-S-H gel.

3.1.3.4 ^{87}Sr MAS NMR

The ^{87}Sr MAS NMR data for the OH_5 sample after curing for 3 days are shown in Figure 3, across the full spectral width obtained, along with the ^{87}Sr MAS NMR data for the NO_3_5 and SO_4_5 samples for comparison (despite numerous attempts ^{87}Sr MAS NMR data was not able to be obtained for the CO_3_5 sample). The ^{87}Sr NMR data each of these samples shows a single resonance with a broad quadrupolar lineshape centred at ~ δ_{obs} = -45 ppm to -65 ppm, with a full width at half maximum (FWHM) on the order of ~ 5 kHz. ^{87}Sr MAS NMR data are very difficult to obtain [29], particularly for disordered materials, however the data obtained here exhibit chemical shifts and FWHM that are broadly consistent with ^{87}Sr MAS NMR data obtained previously for $Sr(NO_3)_2$, $SrSO_4$, and strontium silicate compounds [28, 29].

The ^{87}Sr NMR data for the OH_5 sample after curing for 3 days are shown in Figure 4 across a smaller spectral width focused on the obtained signal. The data exhibit a single resonance with a broad quadrupolar lineshape, centred at δ_{obs} = -63ppm. The low solubility of $Sr(OH)_2{\cdot}8H_2O$ in the activating solution, and observations in the XRD data discussed above, suggest that this is potentially due to $Sr(OH)_2{\cdot}8H_2O$ [18]. The crystalline structure of $Sr(OH)_2$ is tetragonal, where each Sr atom is surrounded by 8 water molecules [47, 48]. The central Sr^{2+} ion is coordinated into an antiprism configuration by 8 oxygen (O) atoms by the H_2O molecules [49]. If the Sr^{2+} cations in these samples are bonded into the geopolymer, it is likely that the formation of a pseudo-zeolite will occur, similar to that of brewsterite, a natural strontium containing zeolite [25]. This hypothesis is supported by the literature, suggesting that similar zeolitic phases form within geopolymer structures after the inclusion of different cations [50, 51]. The structure of this is chemically distinct to that of the crystalline $Sr(OH)_2$, where each of the Sr atoms are bonded to four framework O atoms and five H_2O molecules [52, 53]. Additionally, if Sr^{2+} cations in these samples are bonded into the geopolymer aluminosilicate framework they are expected to exist in a brewsterite-type local structure [25, 50, 51], which may exhibit some similarities in shielding of the ^{87}Sr nuclei to the $SrSiO_3$ phase observed in nuclear waste glasses. The latter has been observed to exhibit an ^{87}Sr MAS NMR resonance at δ_{iso} = 0 ppm [54]. The ^{87}Sr MAS NMR data shown in Figure 4 do not exhibit intensity in this region, and no additional resonances are clearly observed in the data.

View Article Online
DOI: 10.1039/D6DT00775A

Open Access Article. Published on 17 June 2026. Downloaded on 6/17/2026 11:56:12 PM.
This article is licensed under a Creative Commons Attribution 3.0 Unported Licence.

Dalton Transactions Accepted Manuscript

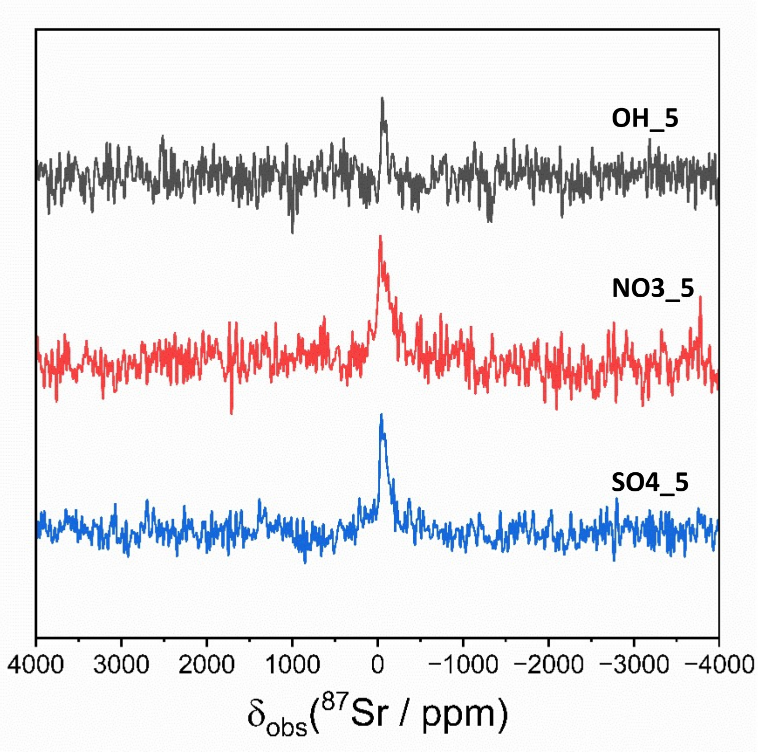

Figure 3: ^{87}Sr MAS NMR data (B_0 = 20.0 T, ν_R = 12.5 kHz, with 1024 data points transformed (out of 8192 data points obtained) and line broadening of 100 Hz applied) for the OH_5, NO3_5 and SO4_5 geopolymer samples cured for 3 days, showing the full spectral width acquired.

View Article Online
DOI: 10.1039/D6DT00775A

Open Access Article. Published on 17 June 2026. Downloaded on 6/17/2026 11:56:12 PM.
This article is licensed under a Creative Commons Attribution 3.0 Unported Licence.

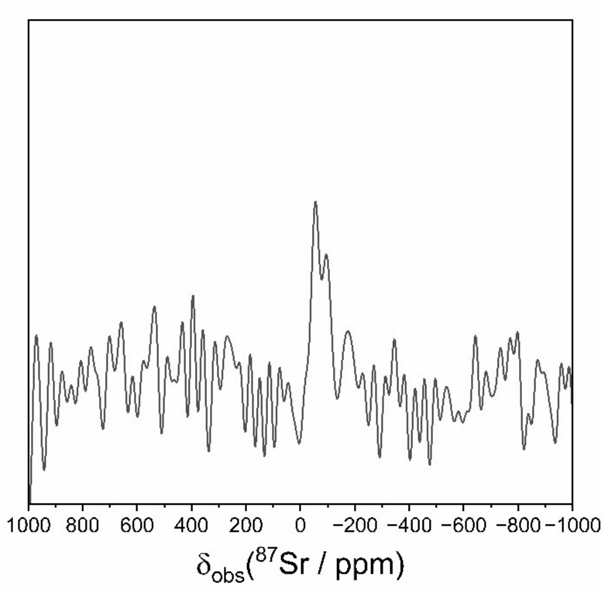

Figure 4: ^{87}Sr MAS NMR data (B_0 = 20.0 T, ν_R = 12.5 kHz, with 1024 data points transformed (out of 8192 data points obtained) and line broadening of 100 Hz applied) for the OH_5 geopolymer sample.

3.1.4 X-ray absorption near-edge structure (XANES) spectroscopy

The normalised spectra for the Sr K-edge XAS analysis of the OH_5 sample after 3 days of reaction compared to both the $Sr(OH)_2{\cdot}8H_2O$ reagent and the mineral brewsterite-Sr ($(Sr,Ba)_2Al_4Si_{12}O_{32}{\cdot}10H_2O$) are shown in Figure 5 [53].

Dalton Transactions Accepted Manuscript

View Article Online
DOI: 10.1039/D6DT00775A

Open Access Article. Published on 17 June 2026. Downloaded on 6/17/2026 11:56:12 PM.
This article is licensed under a Creative Commons Attribution 3.0 Unported Licence.

Dalton Transactions Accepted Manuscript

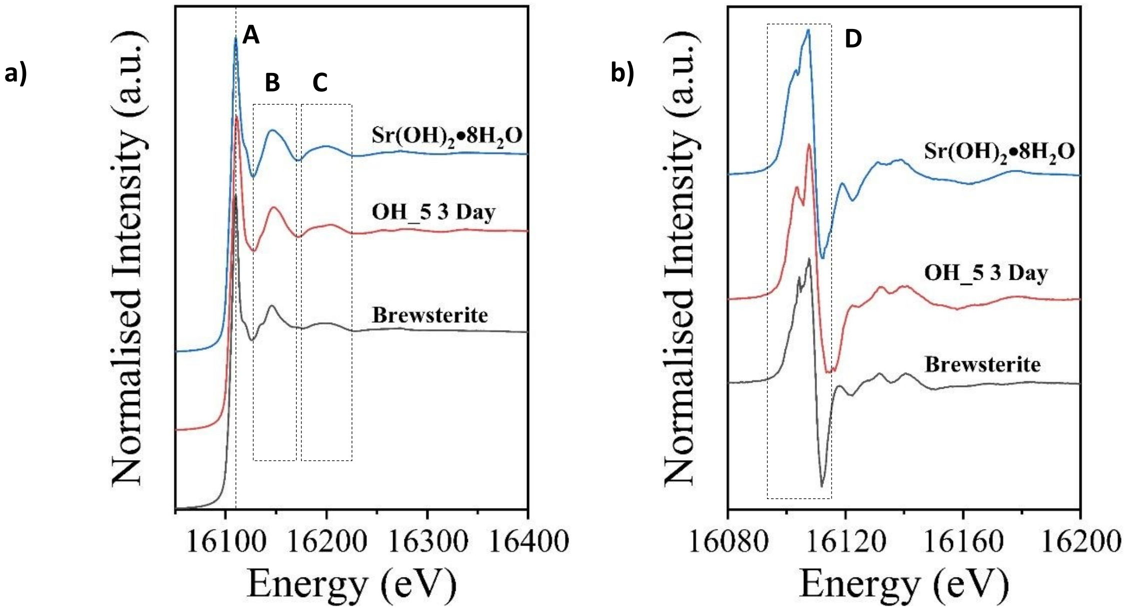

Figure 5: a) Normalised X-ray absorption spectra for the geopolymer samples cured for 3d with $Sr(OH)_2{\cdot}8H_2O$, the $Sr(OH)_2{\cdot}8H_2O$ reactant used, and the mineral brewsterite-Sr, and b) the 1st derivative of these spectra.

The Sr K-edge is relatively featureless, but the highlighted regions in Figure 5 allow for some qualitative analysis between samples [55-57]. When inspecting Figure 5b, the presence of the doublet on the rising edge is observed. This feature is highlighted by the box labelled D in Figure 5 b), and is far more pronounced in the brewsterite-Sr mineral than in the $Sr(OH)_2{\cdot}8H_2O$ reagent. Additionally, when comparing this to the OH_5 sample, the peak is more resembling of the brewsterite spectra than the $Sr(OH)_2{\cdot}8H_2O$ salt, but still displays features of both, most notably the difference in maximums between the two peaks which is more resemblant of the salt. To build upon this, referring back to Figure 5 a), the OH_5 sample appears to exhibit further features of both the salt and Sr in a pseudo-zeolitic structural environment. When exploring the features above the absorption edge, it can be seen that within feature B, the OH_5 sample appears to have a small shoulder at ~ 16135 eV, which is at the same energy as that of the shoulder in the brewsterite spectra. However, this exact same peak follows a similar path to that of the corresponding peak in the $Sr(OH)_2{\cdot}8H_2O$ spectra. Furthermore, feature C for the OH_5 sample appears to show features relating to both the $Sr(OH)_2{\cdot}8H_2O$ reagent and brewsterite, with the lower energy region of this area following a curve comparable to that of brewsterite and the higher energy region comparing to the $Sr(OH)_2{\cdot}8H_2O$ reagent.

View Article Online
DOI: 10.1039/D6DT00775A

From this data, it is implied that the OH_5 sample contains Sr environments both in pseudo-zeolitic structural environments, i.e. incorporated as the charge balancing cation in the K-A-S-H gel, and also in the structural environment of $Sr(OH)_2 \cdot 8H_2O$. This finding is supported by the Sr NMR data, which suggests that there are two Sr environments present within the sample.

3.1.5 Electron probe microanalysis

EPMA images of the OH_5 sample cured for 28 days are shown in Figure 6, and the data exhibit a distribution of Al, Si, and K consistent with the amorphous K-A-S-H gel framework. Unreacted metakaolin particles are observed as Al-rich (dark red) areas, often correlating with Ti-rich regions arising due to the presence of anatase as an impurity in the metakaolin used (identified by XRD and discussed above). Porosity is visible as dark blue regions. Sr appears uniformly distributed as small discrete particles, suggesting it does not dissolve fully in the activating solution and acts primarily as a filler in the geopolymer sample, becoming physically embedded within the matrix. This supports previous observations using isothermal calorimetry and FTIR, which found that the low solubility of $Sr(OH)_2 \cdot 8H_2O$ in the alkali activating solution resulted in limited dissolution of the salt [18]. Some regions have slightly higher Sr concentration, likely due to larger salt particles. K occupies charge-balancing sites within the alkali aluminosilicate framework, and is distributed widely throughout the sample, with regions exhibiting low concentration of K aligning with regions attributed to unreacted metakaolin particles.

Open Access Article. Published on 17 June 2026. Downloaded on 6/17/2026 11:56:12 PM.
This article is licensed under a Creative Commons Attribution 3.0 Unported Licence.

Dalton Transactions Accepted Manuscript

View Article Online
DOI: 10.1039/D6DT00775A

Open Access Article. Published on 17 June 2026. Downloaded on 6/17/2026 11:56:12 PM.
This article is licensed under a Creative Commons Attribution 3.0 Unported Licence.

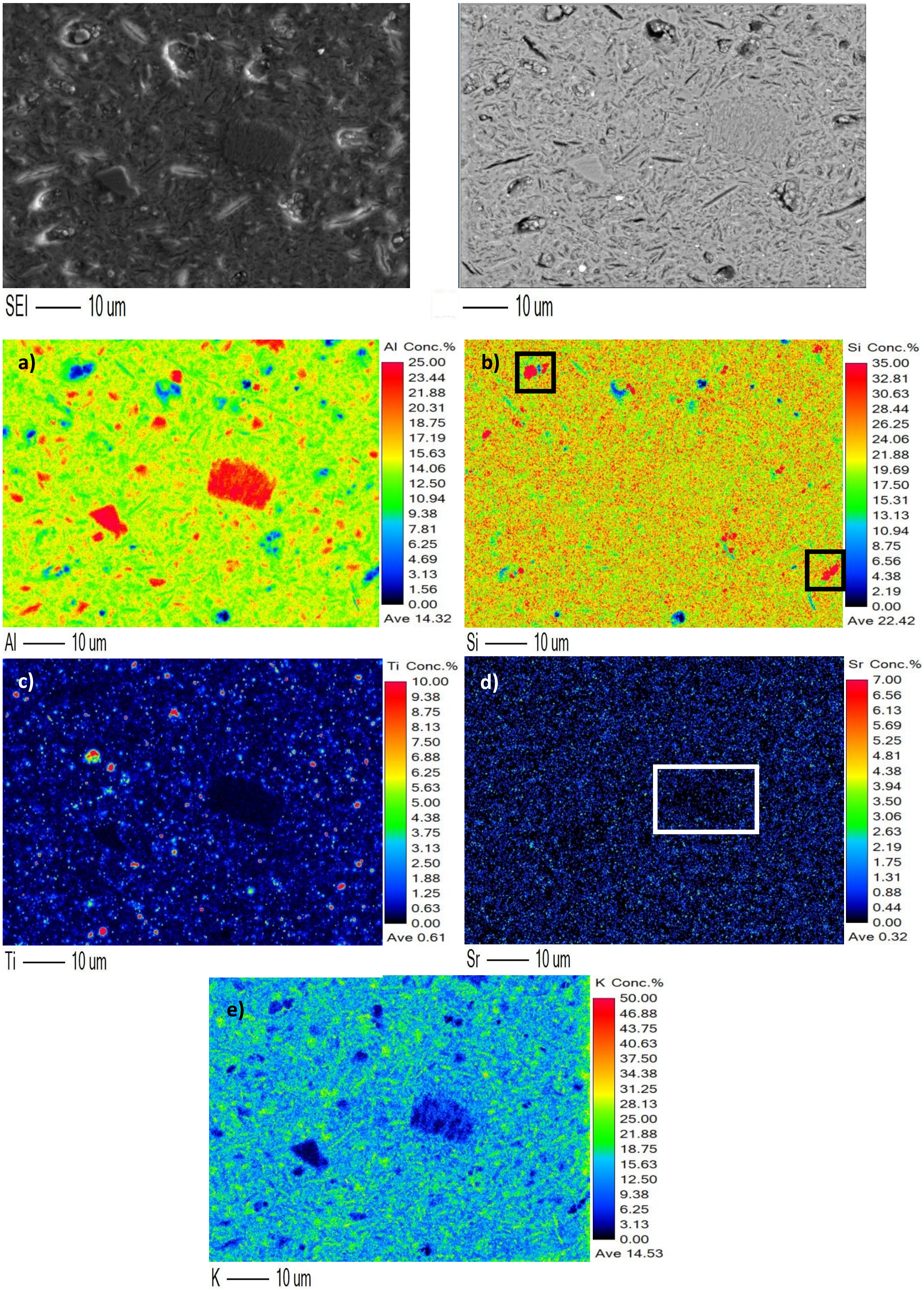

Dalton Transactions Accepted Manuscript

View Article Online
DOI: 10.1039/D6DT00775A

Open Access Article. Published on 17 June 2026. Downloaded on 6/17/2026 11:56:12 PM.
This article is licensed under a Creative Commons Attribution 3.0 Unported Licence.

Figure 6: Electron probe microanalysis images generated for the OH_5 geopolymer for 28 days showing distribution of a) aluminium, b) silicon, c) titanium, d) strontium, and e) potassium within the sample.

Dalton Transactions Accepted Manuscript

View Article Online
DOI: 10.1039/D6DT00775A

Open Access Article. Published on 17 June 2026. Downloaded on 6/17/2026 11:56:12 PM.
This article is licensed under a Creative Commons Attribution 3.0 Unported Licence.

Dalton Transactions Accepted Manuscript

3.2 Effect of addition of strontium carbonate to geopolymers

3.2.1 Fourier transform infrared spectroscopy

FTIR data for the geopolymers incorporating $SrCO_3$ and cured for 3 and 28 days are shown in Figure S3, Supporting Information. The data are very similar to those obtained for geopolymers incorporating $Sr(OH)_2 \cdot 8H_2O$, with a dominant band due to asymmetric stretching of Si-O-T bonds (T = Si or Al) within the K-A-S-H gel [33]. A shoulder at approximately 1050–1100 cm^{-1} indicates the presence of unreacted metakaolin, and bands at 1480 cm^{-1}, 700 cm^{-1}, and 855 cm^{-1} arise due to asymmetric stretching vibrations of CO_3^{2-} anions in $SrCO_3$ [37], indicating the presence of $SrCO_3$ within the geopolymer after 28 days of reaction. Comparing the FTIR data for samples with different Sr/Al ratios, the intensity of the bands arising due to the presence of $SrCO_3$ increase with increasing Sr/Al ratio, corroborating this assignment. This indicates that $SrCO_3$ does not dissolve fully within the activating solution and resides in its solid form within the pores of the gel; $SrCO_3$ has a solubility limit of 0.00034g/100g of H_2O and this reduces as alkalinity increases [58]. The characteristic Si-O-T band does not shift with Sr addition, implying limited structural incorporation of Sr [22, 25]. After curing for 28 days, the main difference in the data compared to that for the sample cured for 3 days is the decreased intensity of the shoulder on the main Si-O-T band due to unreacted metakaolin, indicating continued reaction but no new bond formation.

3.2.2 X-ray diffraction

The X-ray diffraction data for the geopolymer samples containing $SrCO_3$ and cured for 3 and 28 days are shown in Figure S4, Supporting Information. The data show the same features as the XRD data for the geopolymer samples containing $Sr(OH)_2 \cdot 8H_2O$, with a broad feature between 22° 2θ and 35° 2θ, arising from diffuse scattering and consistent with the presence of a K-A-S-H gel [39], as well as reflections due to anatase (TiO_2, PDF # 01-084-1286) which is present as an impurity in the metakaolin used, and reflections due to strontianite ($SrCO_3$, PDF # 00-005-0418). This is consistent with the FTIR data for these samples, and corroborates the interpretation that $SrCO_3$ exhibits low solubility in these samples.

View Article Online
DOI: 10.1039/D6DT00775A

Open Access Article. Published on 17 June 2026. Downloaded on 6/17/2026 11:56:12 PM.
This article is licensed under a Creative Commons Attribution 3.0 Unported Licence.

Dalton Transactions Accepted Manuscript

3.2.3 Solid state nuclear magnetic resonance spectroscopy

3.2.3.1 ^{29}Si MAS and ^{1}H-^{29}Si CP MAS NMR

The ^{1}H -^{29}Si CP MAS NMR and ^{29}Si MAS NMR data for the CO$_3$_5 and KGP samples cured for 3 and 28 days are shown in Figure 7. The ^{1}H-^{29}Si CP MAS NMR data for each geopolymer exhibits a broad resonance centred at δ_{iso} = -85.0 ppm and spanning from δ_{iso} = -75 to -100 ppm, with a consistent lineshape for all samples. Deconvolution and quantification of the ^{1}H-^{29}Si CP MAS and ^{29}Si MAS NMR data (Table S2, Supporting Information) identifies Q^4(4Al), Q^4(3Al), Q^4(2Al), and Q^4(1Al) sites within an Al-rich ($Si/Al \leq 1.2$), fully polymerised K-A-S-H gel [20, 30], with Si/Al ratios similar to that observed for geopolymers incorporating Sr(OH)$_2$.8H$_2$O. The CO$_3$_5 sample shows consistently higher Si/Al ratios than KGP at both time points, which may arise from a lower extent of reaction and hence greater proportion of Si sites from unreacted metakaolin in these samples compared to the control samples. This is consistent with the FTIR and XRD data for these samples, as well as previous observations by isothermal calorimetry [18]. The addition of SrCO$_3$ to the geopolymer system reduces both the reaction rate and the extent of reaction (i.e., the total heat evolved is lower, as observed previously by isothermal calorimetry) compared to the control geopolymer sample. Because SrCO$_3$ is poorly soluble under the high-pH conditions used, many particles remain undissolved and therefore act like an inert filler. This means there is effectively less reactive material (metakaolin + activator) per unit volume, and the reactive surface area is reduced. This reduces the rate of reaction. The calculated extent of reaction shows that the metakaolin precursor continues to react between 3 and 28 days curing.

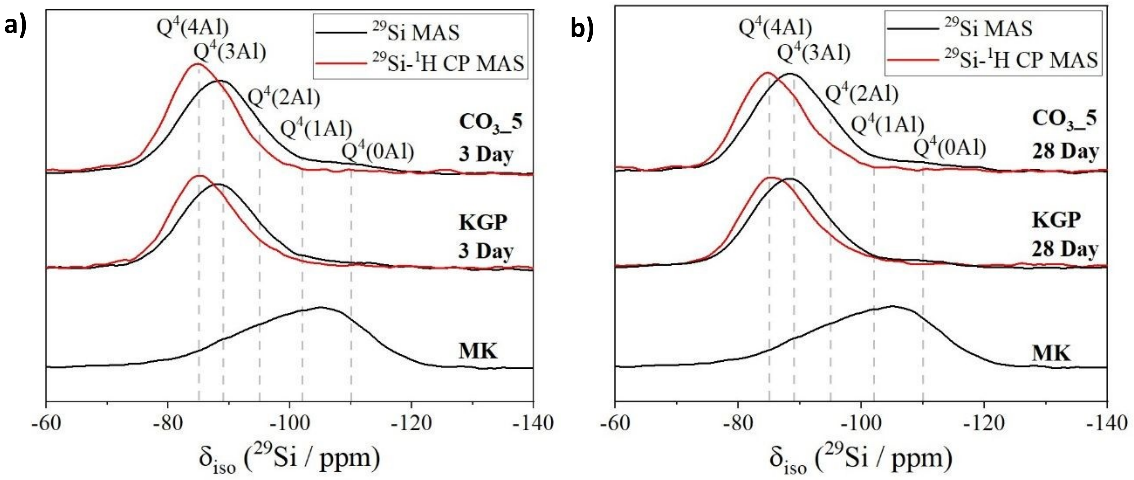

View Article Online
DOI: 10.1039/D6DT00775A

Figure 7: a) ^{1}H-^{29}Si CP MAS (shown in red, B_0 = 11.7 T, ν_R = 12.5 kHz and Hartmann-Hahn contact period t = 2.0 ms) and b) ^{29}Si MAS (shown in black, B_0 = 11.7 T, ν_R = 12.5 kHz) NMR data and associated deconvolutions for geopolymers cured for 3 and 28 days with and without $SrCO_3$, and metakaolin.

3.2.3.2 ^{27}Al and ^{39}K MAS NMR

^{27}Al and ^{39}K MAS NMR data for all samples (Figure 8) are nearly identical to those obtained for geopolymers samples incorporating $Sr(OH)_2.8H_2O$, indicating that Al exists within tetrahedral (q^4) sites in the K-A-S-H type gel as well as octahedral Al sites within remnant unreacted metakaolin, and K exists in charge-balancing extra-framework sites within the K-A-S-H-type gel [19, 44]. This is supported by the findings of both the ^{29}Si MAS and ^{1}H-^{29}Si CP MAS NMR data for these samples. No differences in either resonance are observed when comparing samples with and without Sr.

Open Access Article. Published on 17 June 2026. Downloaded on 6/17/2026 11:56:12 PM.
This article is licensed under a Creative Commons Attribution 3.0 Unported Licence.

Dalton Transactions Accepted Manuscript

a)

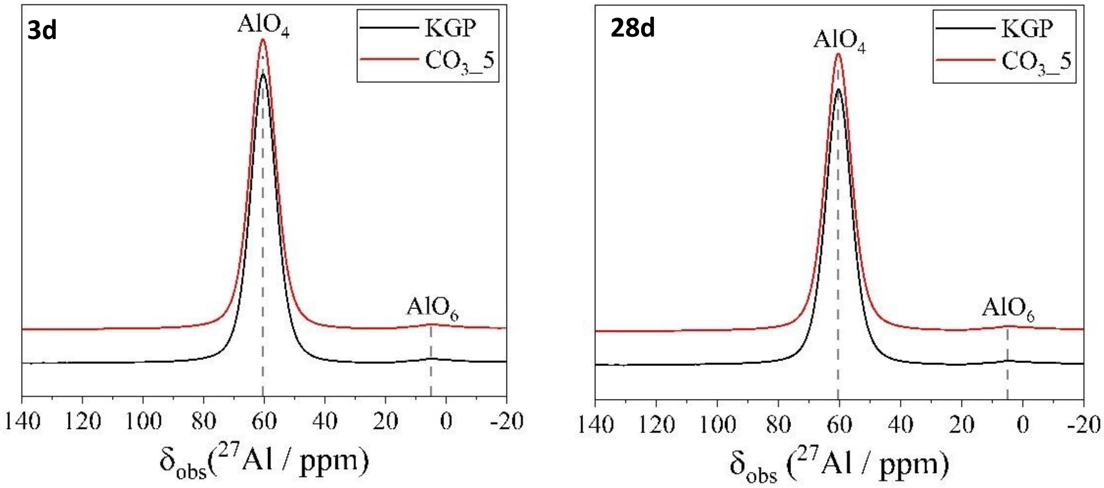

28d

View Article Online
DOI: 10.1039/D6DT00775A

Open Access Article. Published on 17 June 2026. Downloaded on 6/17/2026 11:56:12 PM.
This article is licensed under a Creative Commons Attribution 3.0 Unported Licence.

Dalton Transactions Accepted Manuscript

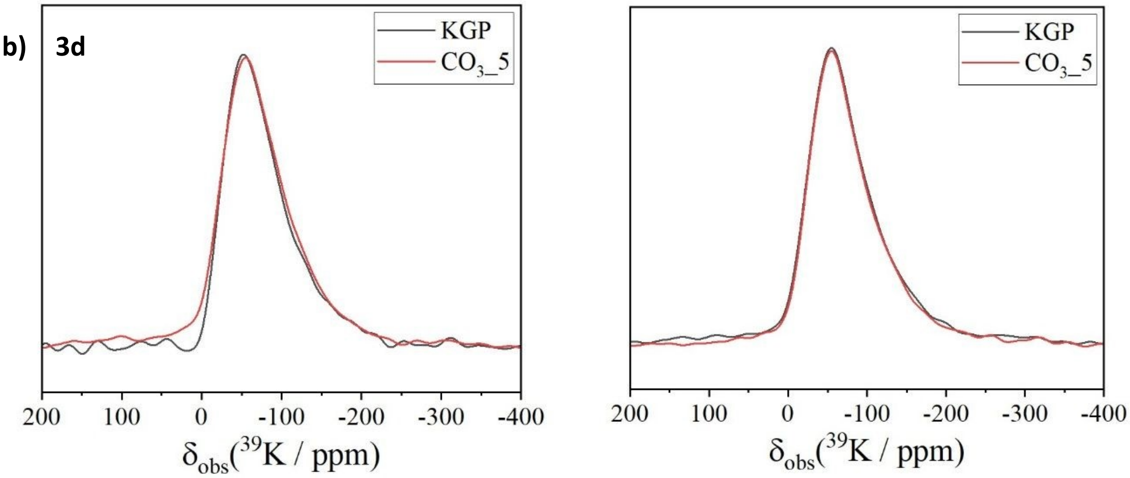

Figure 8: a) ^{27}Al (B_0 = 11.7 T, ν_R = 12.5 kHz) and b) ^{39}K MAS NMR data (B_0 = 20.0 T, ν_R = 12.5 kHz) for each geopolymer cured for with and without $SrCO_3$.

3.2.4 X-ray absorption near-edge structure (XANES) spectroscopy

The normalised spectra for the Sr K-edge XAS analysis of the CO_3_5 sample after 3 and 28 days of reaction compared to both the $SrCO_3$ reagent and brewsterite-Sr ($(Sr,Ba)_2Al_4Si_{12}O_{32}\cdot 10H_2O$) are shown in Figure 9 [53]. The Sr K-edge here displays an absorption edge that rises smoothly to a maximum featuring a singular peak. The Sr K-edge is relatively featureless but provides enough information for a qualitative analysis to be performed. Firstly, the peak maximum, labelled A in Figure 9a), of the brewsterite spectra is reached at slightly lower energies to that of the $SrCO_3$ reagent and the CO_3_5 samples at both time points. This peak appears to be singular in this figure, however, the utilisation of the 1st derivative figure, shown in Figure 9b), shows that there is a very shallow shoulder on the edge. The highlighted region of Figure 9b), labelled D, shows that this doublet peak in the 1st derivative data is more pronounced in the $SrCO_3$ when compared to the brewsterite, and that both of the CO_3_5 samples show similarities with the $SrCO_3$ salt spectra in this region. In addition, referring back to Figure 9a), the features in both highlighted region B and C appear to confirm that the majority of the Sr environments within the CO_3_5 samples at both time points correspond to those of the Sr in $SrCO_3$. There does not seem to be any difference between the spectra for the CO_3_5 samples at 3 and 28 days post reaction. The qualitative analysis performed here indicates that the Sr resides within the sample in the form $SrCO_3$. This is supported by FTIR, XRD, and MAS NMR data discussed above.

View Article Online
DOI: 10.1039/D6DT00775A

Open Access Article. Published on 17 June 2026. Downloaded on 6/17/2026 11:56:12 PM.
This article is licensed under a Creative Commons Attribution 3.0 Unported Licence.

Dalton Transactions Accepted Manuscript

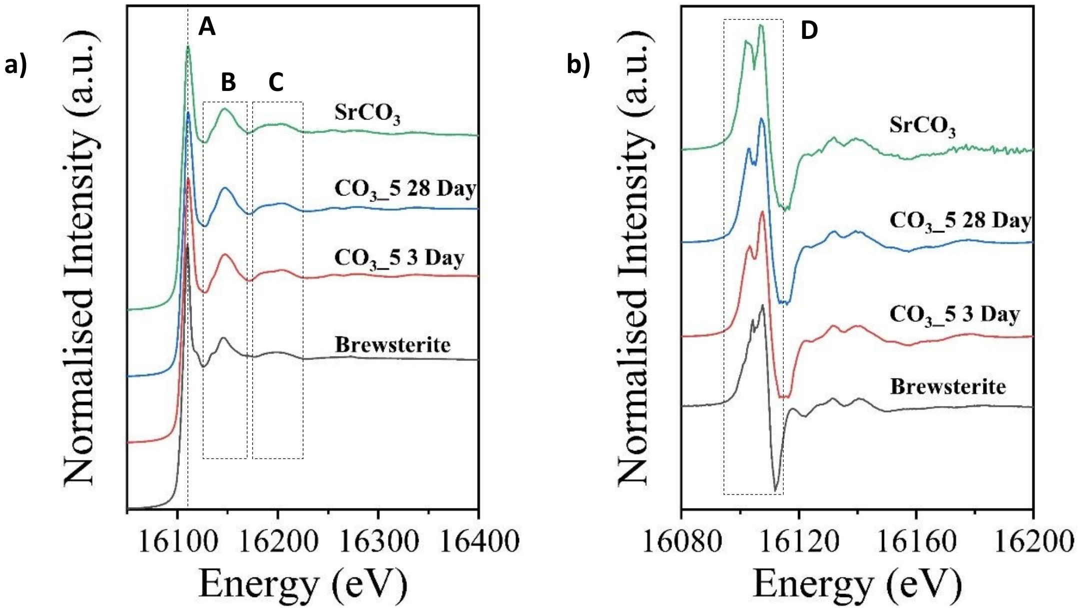

Figure 9: a) Normalised X-ray absorption spectra for the geopolymer samples loaded with $SrCO_3$, reagent grade $SrCO_3$, and the mineral brewsterite-Sr, and b) the 1st derivative of these spectra.

3.2.5 Electron probe microanalysis

EPMA images of the CO_3_5 sample cured for 28 days are shown in Figure 10, and the data exhibit a distribution of Al, Si, and K consistent with the amorphous K-A-S-H gel framework. Similar to the data for geopolymers incorporating $Sr(OH)_2·8H_2O$, the data show unreacted metakaolin particles (observed as Al-rich regions), also correlating with Ti-rich regions arising due to the presence of anatase as an impurity in the metakaolin used. Sr is located in discrete particles or clusters of particles a few microns in diameter, contrasting with the observations for geopolymers incorporating of $Sr(OH)_2·8H_2O$ which showed Sr was uniformly distributed throughout the samples is sub-micron particles. This indicates that Sr in geopolymers incorporating of $SrCO_3$ exists in discrete $SrCO_3$ particles, consistent with its low solubility within these samples. K occupies charge-balancing sites within the alkali aluminosilicate framework, and is distributed widely throughout the sample, with regions exhibiting low concentration of K align with regions attributed to unreacted metakaolin particles.

View Article Online
DOI: 10.1039/D6DT00775A

Open Access Article. Published on 17 June 2026. Downloaded on 6/17/2026 11:56:12 PM.
This article is licensed under a Creative Commons Attribution 3.0 Unported Licence.

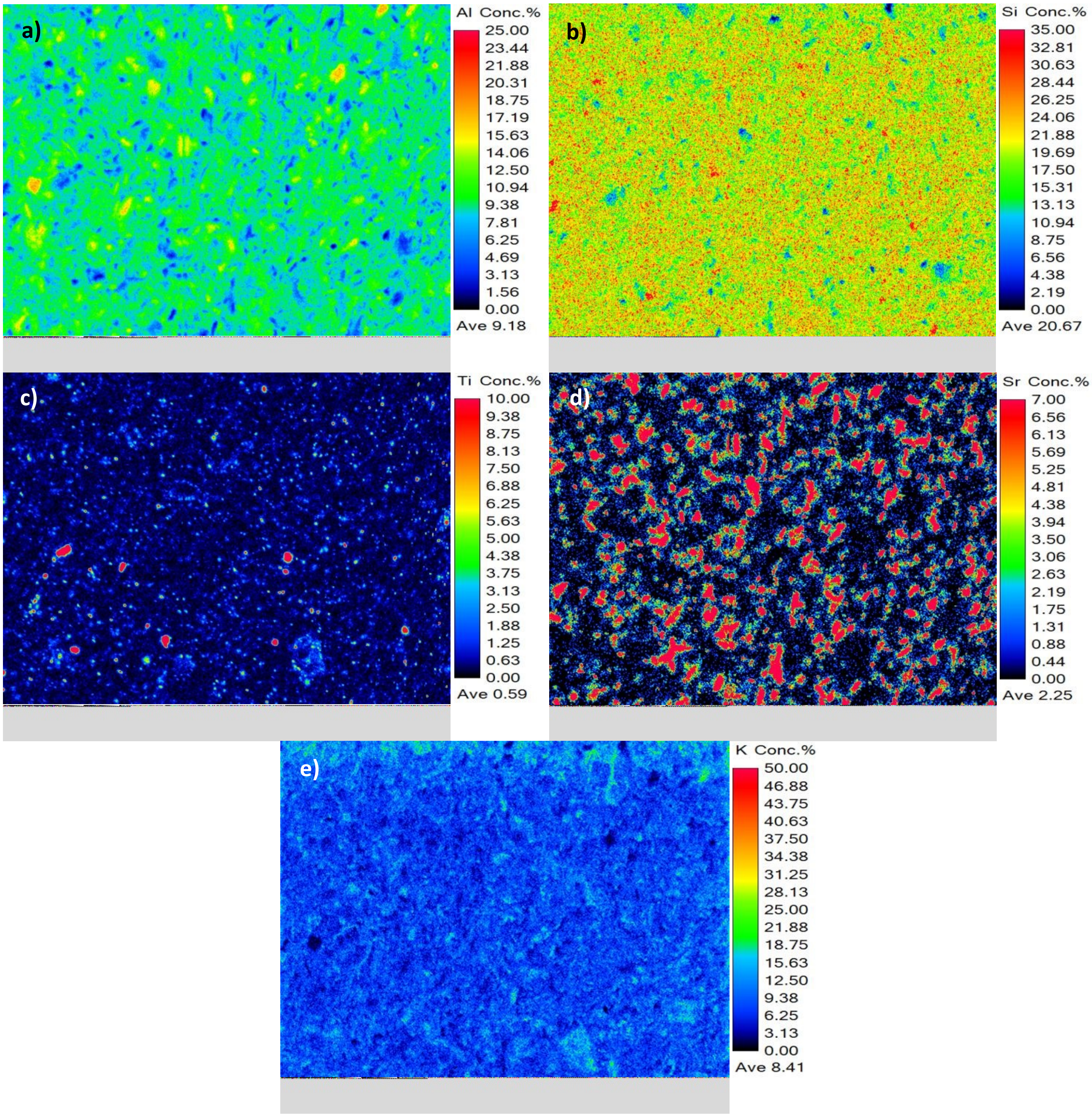

Figure 10: Electron probe microanalysis images generated for the CO_3_5 geopolymer for 28 days showing distribution of a) aluminium, b) silicon, c) titanium, d) strontium, and e) potassium within the sample.

Dalton Transactions Accepted Manuscript

View Article Online
DOI: 10.1039/D6DT00775A

Open Access Article. Published on 17 June 2026. Downloaded on 6/17/2026 11:56:12 PM.
This article is licensed under a Creative Commons Attribution 3.0 Unported Licence.

Dalton Transactions Accepted Manuscript

3.3 Effect of addition of strontium nitrate to geopolymers

3.3.1 Fourier transform infrared spectroscopy

FTIR data for the geopolymers incorporating $Sr(NO_3)_2$ and cured for 3 and 28 days are shown in Figure S5, Supporting Information. The data are very similar to those obtained for geopolymers incorporating $Sr(OH)_2 \cdot 8H_2O$ and $SrCO_3$, with a dominant band due to asymmetric stretching of Si-O-T bonds (T = Si or Al) within the K-A-S-H gel [33] and a shoulder at approximately 1050–1100 cm^{-1} indicating the presence of unreacted metakaolin. Vibrational bands at 1385 cm^{-1} and at 825 cm^{-1} are attributed to vibrations in NO_3^- ions in $Sr(NO_3)_2$ and KNO_3, indicating that $Sr(NO_3)_2$ has dissolved to some extent, and the subsequent reaction in the aqueous phase has resulted in formation and precipitation of KNO_3, and that some unreacted $Sr(NO_3)_2$ is also present within these samples after 28 days of reaction. Comparing the FTIR data for samples with different Sr/Al ratios, the intensity of the bands arising due to the presence of $Sr(NO_3)_2$ and KNO_3 increase with increasing Sr/Al ratio, corroborating this assignment.

3.3.2 X-ray diffraction

The X-ray diffraction data for the geopolymer samples containing $Sr(NO_3)_2$ and cured for 3 and 28 days are shown in Figure S6, Supporting Information. The data show a broad feature between 22° 2θ and 35° 2θ, arising from diffuse scattering and consistent with the presence of a K-A-S-H gel [39], as well as reflections due to anatase (TiO_2, PDF # 01-084-1286) which is present as an impurity in the metakaolin used. The data also contain reflections due to niter (KNO_3, PDF # 01-071-1558) suggests that the NO_3^- ions in solution due to the dissolution of the $Sr(NO_3)_2$ are reacting with the aqueous K^+ ions forming KNO_3. The observation of low intensity reflections due to strontianite ($SrCO_3$, PDF # 00-005-0418) indicates that some of the dissolved Sr^{2+} is reacting with dissolved carbonic acid (H_2CO_3), itself arising from dissolution of atmospheric CO_2 in the pore solution. Together with the FTIR data for these samples, this shows that $Sr(NO_3)_2$ is significantly soluble in the fresh state aqueous phase of these samples.

3.3.3 Solid state nuclear magnetic resonance spectroscopy

3.3.3.1 ^{29}Si MAS and ^{1}H-^{29}Si CP MAS NMR

The ^{1}H -^{29}Si CP MAS NMR and ^{29}Si MAS NMR data for the NO_3_5 and KGP samples cured for 3 and 28 days are shown in Figure 17. The ^{1}H-^{29}Si CP MAS NMR data for each geopolymer exhibits a broad resonance

View Article Online
DOI: 10.1039/D6DT00775A

Open Access Article. Published on 17 June 2026. Downloaded on 6/17/2026 11:56:12 PM.
This article is licensed under a Creative Commons Attribution 3.0 Unported Licence.

Dalton Transactions Accepted Manuscript

centred at δ_{iso} = -85.0 ppm and spanning from δ_{iso} = -75 to -100 ppm, with a consistent lineshape for all samples. Deconvolution and quantification of the ^{1}H-^{29}Si CP MAS and ^{29}Si MAS NMR data identifies Q^4(4Al), Q^4(3Al), Q^4(2Al), and Q^4(1Al) sites within an Al-rich (Si/Al ≤ 1.2), fully polymerised K-A-S-H gel [20, 30], with Si/Al ratios similar to that observed for geopolymers incorporating $Sr(OH)_2.8H_2O$ and $SrCO_3$. The NO_3_5 sample appears to have a gel structure dominated by Q^4(4Al), Q^4(3Al) and Q^4(2Al) silicon sites after 3 days but after 28 days, the percentage of Q^4(2Al) sites drops significantly to a structure dominated by Q^4(4Al) and Q^4(3Al) sites. This shows that the Al content of the K-A-S-H gel is increasing over time, agreeing with the Si/Al ratios shown in Table S3, Supporting Information. Previous work using zeta potential measurements of dispersions of metakaolin particles in solutions representative of the aqueous phase in the fresh geopolymers studied in this work suggest that the dissolution of the metakaolin is slowed due to the adsorption of Sr^{2+} cations to its surface, reducing electrostatic repulsion resulting in particle agglomeration (and hence a lower reactive surface area), forming a Sr^{2+} layer on the surface that physically and electrostatically shields metakaolin from OH^- ions, reducing dissolution of Al/Si species needed to form the K-A-S-H gel [18]. The results here show that this leads to a Si-rich K-A-S-H gel in the early stages of the reaction (due to the presence of excess soluble silica from the activating solution) which becomes more Al-rich as the sample ages. This is consistent with the FTIR and XRD data for these samples, as well as previous observations by isothermal calorimetry [18]. The calculated extent of reaction shows that the metakaolin precursor continues to react between 3 and 28 days curing, however these are lower than when geopolymers are produced in the presence of $Sr(OH)_2.8H_2O$ and $SrCO_3$, consistent with the lower rate of reaction due to the presence of Sr on the surface of metakaolin particles described above [18].

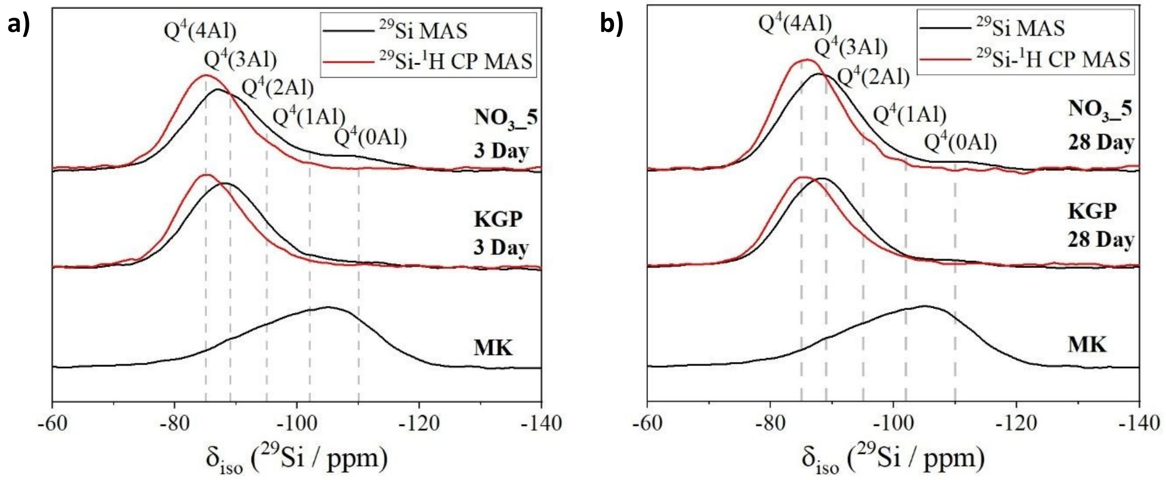

Figure 11: a) ^1H-^{29}Si CP MAS (shown in red, B_0 = 11.7 T, ν_R = 12.5 kHz and Hartmann-Hahn contact period t = 2.0 ms) and b) ^{29}Si MAS (shown in black, B_0 = 11.7 T, ν_R = 12.5 kHz) NMR data and associated deconvolutions for geopolymers cured for 3 and 28d with and without $Sr(NO_3)_2$, and metakaolin.

View Article Online
DOI: 10.1039/D6DT00775A

Open Access Article. Published on 17 June 2026. Downloaded on 6/17/2026 11:56:12 PM.
This article is licensed under a Creative Commons Attribution 3.0 Unported Licence.

3.3.3.2 ^{27}Al and ^{39}K MAS NMR

^{27}Al and ^{39}K MAS NMR data for all samples (Figure 12) are nearly identical to those obtained for geopolymers samples incorporating $Sr(OH)_2.8H_2O$ and $SrCO_3$, indicating that Al exists within tetrahedral (q^4) sites in the K-A-S-H type gel as well as octahedral Al sites within remnant unreacted metakaolin, and K exists in charge-balancing extra-framework sites within the K-A-S-H-type gel [19, 44]. This is supported by the findings of both the ^{29}Si MAS and ^{1}H-^{29}Si CP MAS NMR data for these samples. No differences in either resonance are observed when comparing samples with and without Sr.

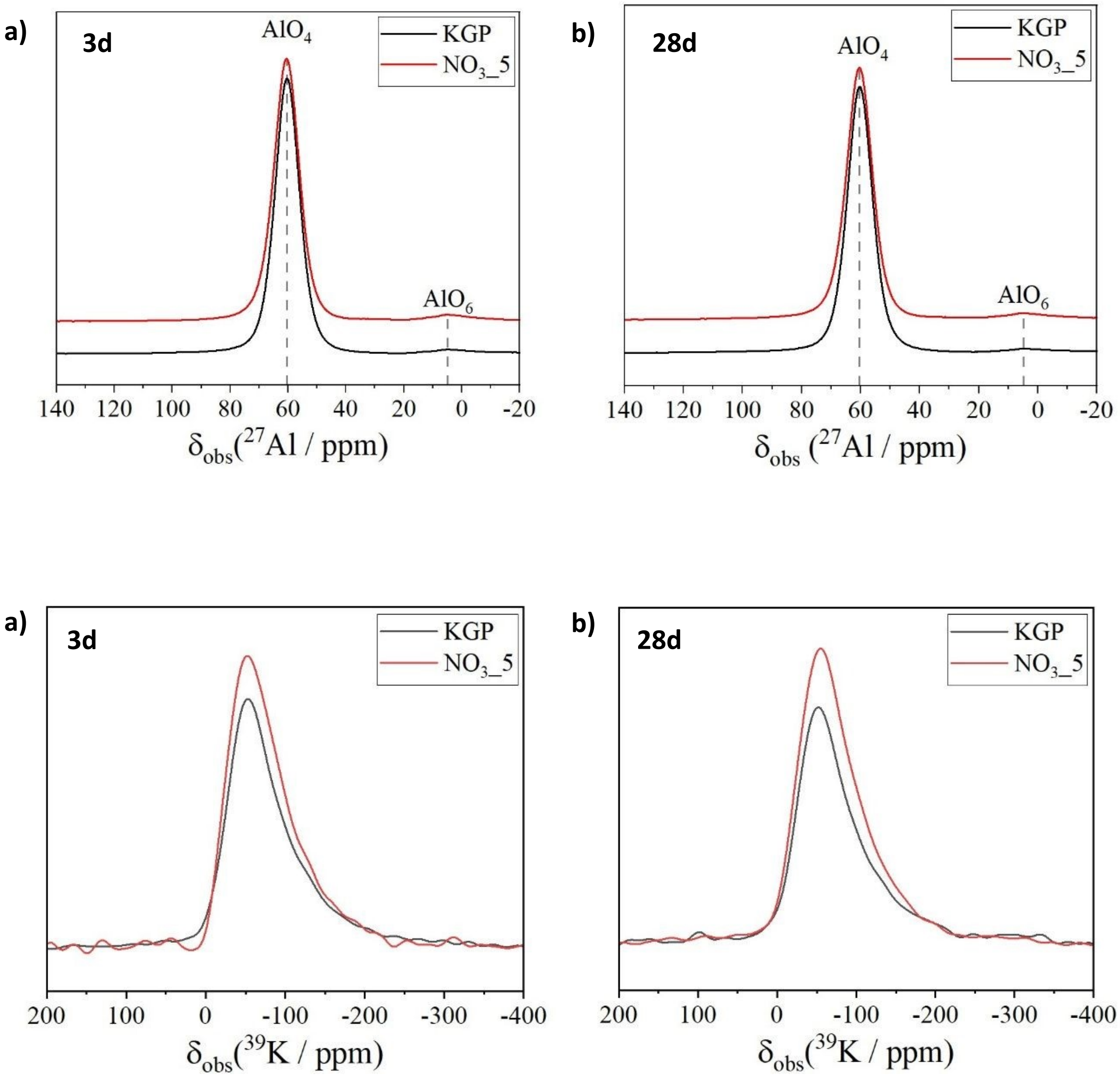

Figure 12: a) ^{27}Al (B_0 = 11.7 T, ν_R = 12.5 kHz) and b) ^{39}K MAS NMR data (B_0 = 20.0 T, ν_R = 12.5 kHz) for each geopolymer cured for 3 and 28d with and without $Sr(NO_3)_2$.

Dalton Transactions Accepted Manuscript

View Article Online
DOI: 10.1039/D6DT00775A

Open Access Article. Published on 17 June 2026. Downloaded on 6/17/2026 11:56:12 PM.
This article is licensed under a Creative Commons Attribution 3.0 Unported Licence.

Dalton Transactions Accepted Manuscript

The ^{87}Sr MAS NMR data for the NO$_3$_5 sample after curing for 3 days are shown in Figure 13. Similar to the data obtained for geopolymers incorporating $Sr(OH)_2 \cdot 8H_2O$, the ^{87}Sr MAS NMR data for the NO$_3$_5 sample after curing for 3 days exhibits a single distinct resonance with a broad quadrupolar lineshape, centred at approximately δ_{obs} = -73 ppm. This is broadly consistent with the chemical shift and FWHM observed for ^{87}Sr MAS NMR data for $Sr(NO_3)_2$ [28], suggesting that this phase may be responsible for the resonance observed in the data here. Additionally, as discussed above, if Sr^{2+} cations in these samples are bonded into the geopolymer aluminosilicate framework they are expected to exist in a brewsterite-type local structure [25, 50, 51], which may exhibit some similarities in shielding of the ^{87}Sr nuclei to the $SrSiO_3$ phase observed in nuclear waste glasses [54]. The latter has been observed to exhibit an ^{87}Sr MAS NMR resonance at δ_{iso} = 0 ppm. The ^{87}Sr MAS NMR data shown in Figure 13 exhibit significant intensity in this region, as a shoulder on the main resonance, however this shoulder is not significantly above the spectral noise, and so no firm conclusions can be drawn from this data about the existence of this site.

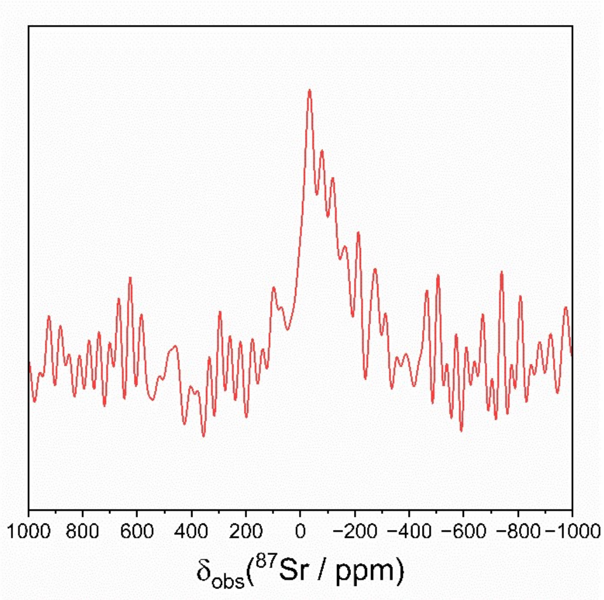

Figure 13: ^{87}Sr MAS NMR data (B_0 = 20.0 T, ν_R = 12.5 kHz with 1024 data points transformed (out of 8192 data points obtained) and line broadening of 100 Hz applied) for the NO$_3$_5 geopolymer sample cured for 3 days with $Sr(NO_3)_2$.

3.3.4 X-ray absorption near-edge structure (XANES) spectroscopy

The normalised spectra for the Sr K-edge XAS analysis of the NO$_3$_5 sample after 3 and 28 days of reaction compared to both the $Sr(NO_3)_2$ reagent and brewsterite-Sr ($(Sr,Ba)_2Al_4Si_{12}O_{32} \cdot 10H_2O$) are shown in Figure

View Article Online
DOI: 10.1039/D6DT00775A

Open Access Article. Published on 17 June 2026. Downloaded on 6/17/2026 11:56:12 PM.
This article is licensed under a Creative Commons Attribution 3.0 Unported Licence.

Dalton Transactions Accepted Manuscript

14 [53]. The XRD data for these samples show that there is a quantity of $SrCO_3$ within the NO_3_5 sample, and so it may be more relevant to compare the XANES spectra to a $SrCO_3$ standard (Figure 14). Firstly, by inspecting the region labelled as B in Figure 14a), the line shape of the spectra for both NO_3_5 samples aligns more closely with the line shape of the $SrCO_3$ standard as opposed to the brewsterite. The shoulder on the peak that is easily seen in the brewsterite spectra cannot be seen so clearly in the spectra for the NO_3_5 samples. Moreover, the feature in region C aligns closely between the $SrCO_3$ and the NO_3_5 samples. The evidence here suggest that the Sr is likely to be mainly found in the form of $SrCO_3$, with smaller quantities of Sr present in a brewsterite-type local structure. Overall, the spectra here suggest that all of the $Sr(NO_3)_2$ dissolves within the activating solution upon its initial addition. The Sr^{2+} cations that are subsequently released into solution are likely to react with the CO_2 in the air to form crystalline $SrCO_3$, which is supported by the XRD and the XANES spectra here.

View Article Online
DOI: 10.1039/D6DT00775A

Open Access Article. Published on 17 June 2026. Downloaded on 6/17/2026 11:56:12 PM.
This article is licensed under a Creative Commons Attribution 3.0 Unported Licence.

Dalton Transactions Accepted Manuscript

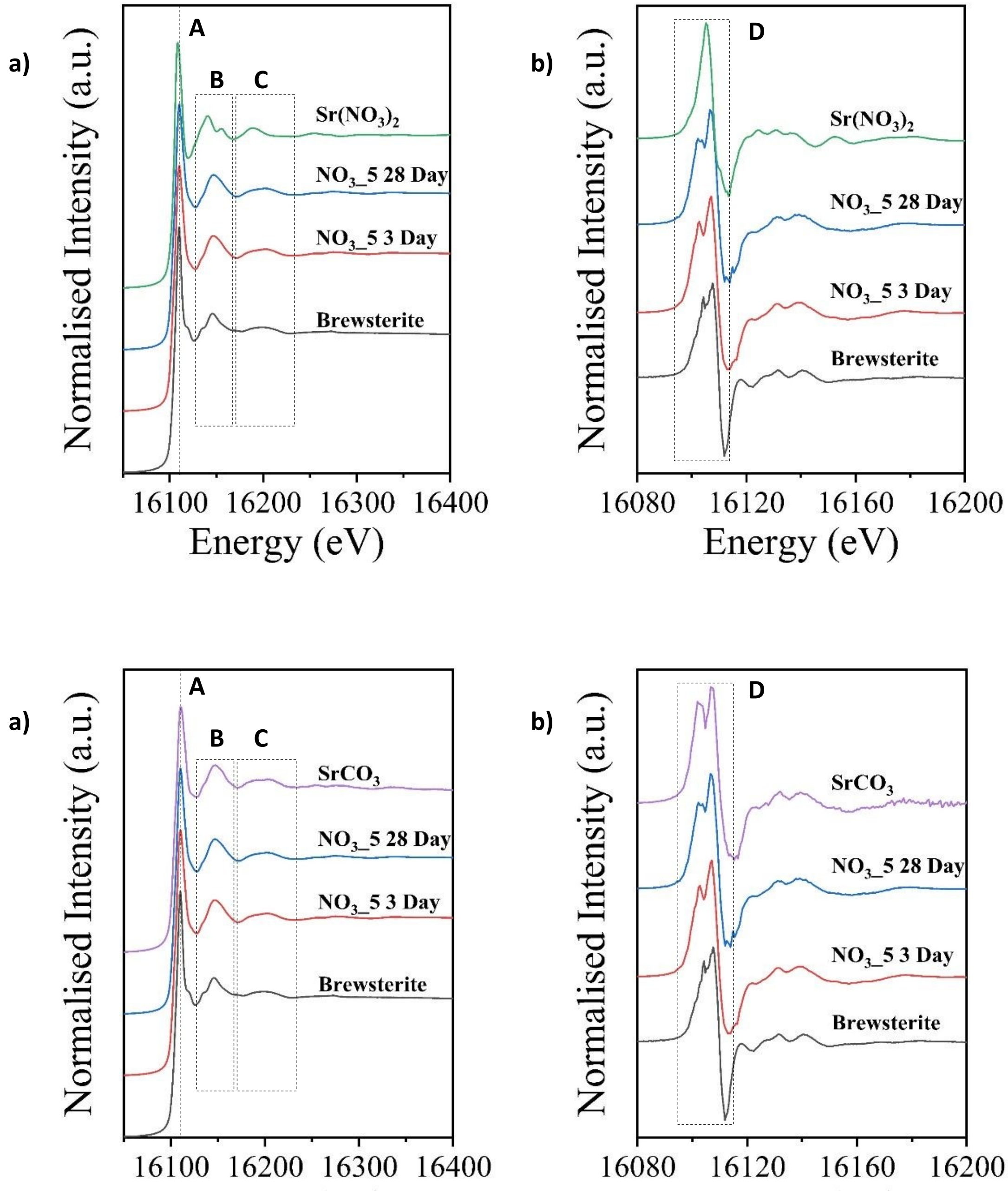

Figure 14: a) Normalised X-ray absorption spectra for the geopolymer samples loaded with Sr(NO$_3$)$_2$, reagent grade Sr(NO$_3$)$_2$, and the mineral brewsterite-Sr, and b) the 1st derivative of these spectra.

3.3.5 Electron probe microanalysis

EPMA images of the NO$_3$_5 sample cured for 28 days are shown in Figure 15, and the data exhibit a distribution of Al, Si, and K consistent with the amorphous K-A-S-H gel framework. Similar to the data for

View Article Online
DOI: 10.1039/D6DT00775A

geopolymers incorporating of $Sr(OH)_2·8H_2O$, the data show unreacted metakaolin particles (observed as Al-rich regions), also correlating with Ti-rich regions arising due to the presence of anatase as an impurity in the metakaolin used. Sr appears uniformly distributed throughout the geopolymer matrix, supporting the possibility that Sr^{2+} is displacing K^+ to act as a charge-balancing cation within the K-A-S-H gel framework (also indicated by XANES data). Furthermore, the concentration of K is also distributed evenly throughout the geopolymer matrix, suggesting that K remains the primary charge-balancing cation.

Open Access Article. Published on 17 June 2026. Downloaded on 6/17/2026 11:56:12 PM.
This article is licensed under a Creative Commons Attribution 3.0 Unported Licence.

Dalton Transactions Accepted Manuscript

View Article Online
DOI: 10.1039/D6DT00775A

Open Access Article. Published on 17 June 2026. Downloaded on 6/17/2026 11:56:12 PM.
This article is licensed under a Creative Commons Attribution 3.0 Unported Licence.

Dalton Transactions Accepted Manuscript

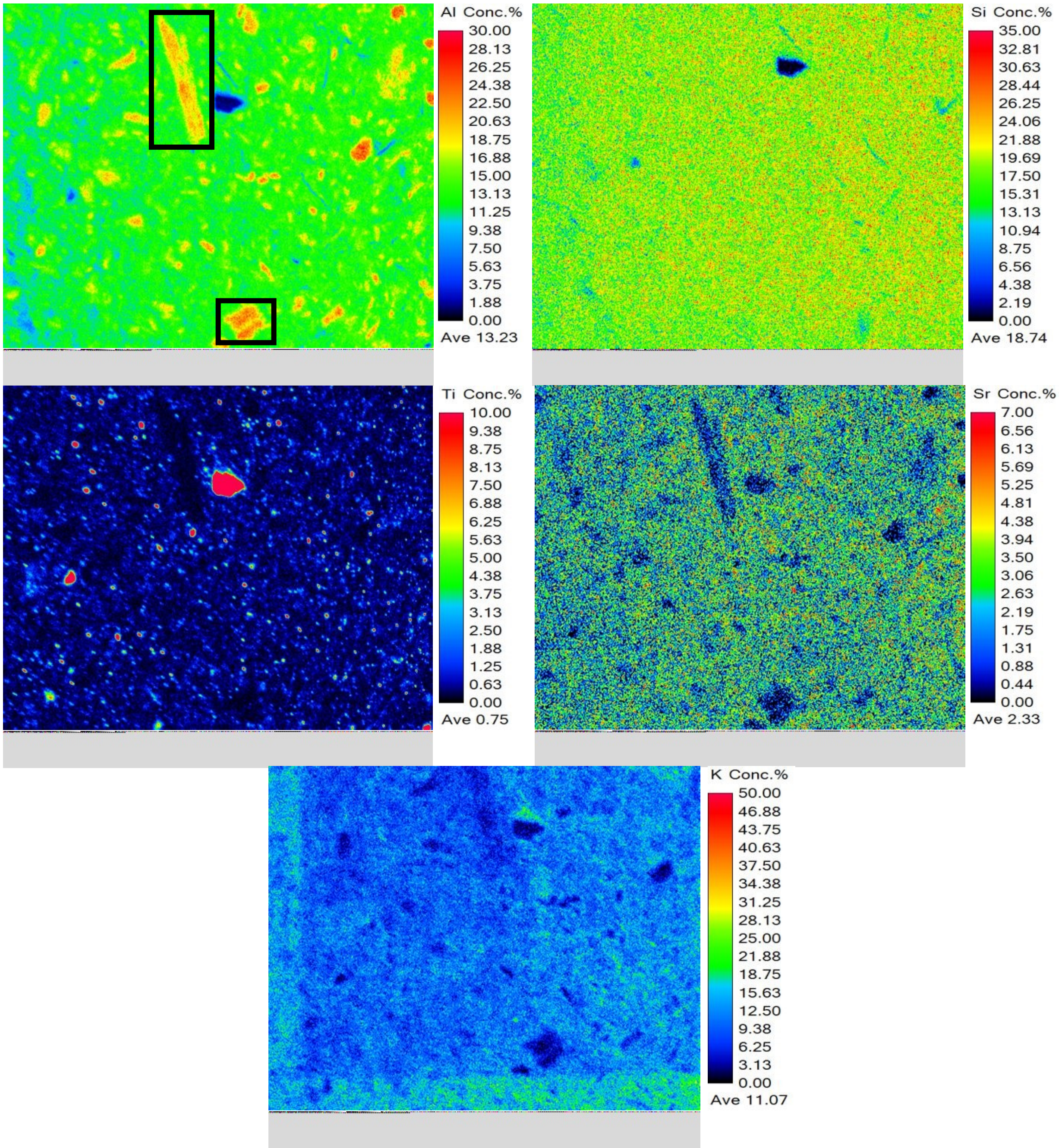

Figure 15: Electron probe microanalysis images generated for the NO_3_5 geopolymer for 28 days showing distribution of a) aluminium, b) silicon, c) titanium, d) strontium, and e) potassium within the sample.

View Article Online
DOI: 10.1039/D6DT00775A

Open Access Article. Published on 17 June 2026. Downloaded on 6/17/2026 11:56:12 PM.
This article is licensed under a Creative Commons Attribution 3.0 Unported Licence.

Dalton Transactions Accepted Manuscript

3.4 Effect of addition of strontium sulfate to geopolymers

3.4.1 Fourier transform infrared spectroscopy

FTIR data for the geopolymers incorporating $SrSO_4$ and cured for 3 and 28 days are shown in Figure S7, Supporting Information. The data are similar to those obtained for geopolymers incorporating $Sr(OH)_2{\cdot}8H_2O$, $SrCO_3$, and $Sr(NO_3)_2$, with a dominant band due to asymmetric stretching of Si-O-T bonds (T = Si or Al) within the K-A-S-H gel [33]. A shoulder at approximately 1050–1100 cm^{-1} indicates the presence of unreacted metakaolin. There are a few noticeable differences between the spectra at 3 days and the spectra at 28 days, most prominently the sharp peaks that are seen at 667 cm^{-1} in the SO_4_1 and SO_4_5 samples. It is possible that these peaks are due to the presence of kalistrontite ($K_2Sr(SO_4)_2$) within the sample, as observed by XRD. The FTIR data appear very similar regardless of the Sr/Al ratio of the samples. This suggests that the K-A-S-H gel structure is not altered by the addition of the $SrSO_4$, as observed by FTIR, despite the clear effects on the kinetics observed previously [18].

3.4.2 X-ray diffraction

The X-ray diffraction data for the geopolymer samples containing $SrSO_4$ and cured for 3 and 28 days are shown in Figure S8, Supporting Information. The data show the same features as the XRD data for the geopolymer samples containing $Sr(OH)_2{\cdot}8H_2O$, with a broad feature between 22° 2θ and 35° 2θ, arising from diffuse scattering and consistent with the presence of a K-A-S-H gel [39], as well as reflections due to anatase (TiO_2, Powder Diffraction file (PDF) # 01-084-1286) which is present as an impurity in the metakaolin used, and reflections due to strontianite ($SrCO_3$, PDF # 00-005-0418). The presence of reflections due to celestine ($SrSO_4$, PDF # 04-009-9879) confirms that not all of the $SrSO_4$ dissolves into the activating solution. The presence of this becomes greater with increasing Sr/Al ratio, suggesting that the solubility limit is reached between the SO_4_1 and SO_4_2 samples. The presence of arcanite (K_2SO_4, PDF #00-024-0703) suggests that the dissolved SO_4^{2-} anions react with the K^+ ions in solution to precipitate a solid, crystalline K_2SO_4 phase. The presence of this also increases with increasing Sr/Al ratio, suggesting that, as more $SrSO_4$ dissolves, there are more SO_4^{2-} anions available to react with the K^+ cations as would be expected. This is similar for the kalistrontite ($K_2Sr(SO_4)_2$, PDF # 04-025-4251), which increases in prominence as mass of $SrSO_4$ in the sample increases. The formation of kalistrontite is not unexpected, as it is seen in the literature that deposits of kalistrontite have been found in the presence of $SrSO_4$ and K-bearing phases [59, 60]. The presence of this crystalline solid could explain the changes seen to the

View Article Online
DOI: 10.1039/D6DT00775A

Open Access Article. Published on 17 June 2026. Downloaded on 6/17/2026 11:56:12 PM.
This article is licensed under a Creative Commons Attribution 3.0 Unported Licence.

Dalton Transactions Accepted Manuscript

reaction kinetics observed previously [18], as $SrSO_4$ is observed to react with the activating solution upon its addition. The crystallisation, and probable resultant precipitation, of this solid, as well as consumption of both K^+ and Sr^{2+}, the two cations within solution that are responsible for the charge balancing of the AlO_4^- sites in the gel phase, may then affect dissolution of metakaolin and formation of the K-A-S-H gel. The presence of reflections due to strontianite ($SrCO_3$, PDF # 00-005-0418) in the XRD data is most likely due to the carbonation of the sample via contact with air. However, there is very little of this compound present within the sample, providing further evidence that there is a minimal amount of excess ‘free’ Sr within the sample, as the majority of it has either not dissolved (remaining as $SrSO_4$), has reacted with the activating solution to form kalistrontite, or has been incorporated into the K-A-S-H gel in place of K. After 28 days, the diffraction patterns show the presence of all of the crystalline phases seen after 3 days. The presence of quartz (SiO_2, PDF # 01-078-2315) is also seen, an inert compound found in the raw metakaolin precursor.

3.4.3 Solid state nuclear magnetic resonance spectroscopy

3.4.3.1 ^{29}Si MAS and ^{1}H-^{29}Si CP MAS NMR

The ^{1}H -^{29}Si CP MAS NMR and ^{29}Si MAS NMR data for the SO_4_5 and KGP samples cured for 3 and 28 days are shown in Figure 16. The ^{1}H-^{29}Si CP MAS NMR data for each geopolymer exhibits a broad resonance centred at δ_{iso} = -85.0 ppm and spanning from δ_{iso} = -75 to -100 ppm, with a consistent lineshape for all samples. Deconvolution and quantification of the ^{1}H-^{29}Si CP MAS and ^{29}Si MAS NMR data identifies Q^4(4Al), Q^4(3Al), Q^4(2Al), and Q^4(1Al) sites within an Al-rich (Si/Al ≤ 1.2), fully polymerised K-A-S-H gel [20, 30], with Si/Al ratios similar to that observed for geopolymers incorporating $Sr(OH)_2.8H_2O$, $SrCO_3$, and $Sr(NO_3)_2$. The SO_4_5 sample shows consistently higher Si/Al ratios than KGP at both time points, which may arise from a lower extent of reaction and hence greater proportion of Si sites from unreacted metakaolin in these samples compared to the control samples. This is consistent with the FTIR and XRD data for these samples, as well as previous observations by isothermal calorimetry [18]. The calculated extent of reaction shows that the metakaolin precursor continues to react between 3 and 28 days curing.

The Si/Al ratio of the SO_4_5 samples after both 3 and 28 days are greater than that of the KGP sample suggesting that the incorporation of $SrSO_4$ at such a high Sr/Al ratio slightly decreases the cation binding capability of the gel. This is contrary to what has been seen in previous work, with Walkley et al. showing that the Si/Al ratio for K-activated geopolymer systems containing Sr is less than the associated control

View Article Online
DOI: 10.1039/D6DT00775A

Open Access Article. Published on 17 June 2026. Downloaded on 6/17/2026 11:56:12 PM.
This article is licensed under a Creative Commons Attribution 3.0 Unported Licence.

Dalton Transactions Accepted Manuscript

geopolymer system [22]. However, this is using much lower concentrations of Sr within the structure, which would have less of an impact on the formation of the K-A-S-H phase.

The SO_4_5 sample appears to have a gel structure dominated by Q^4(4Al), Q^4(3Al) and Q^4(2Al) silicon sites after 3 days but after 28 days, the percentage of Q^4(2Al) sites drops significantly to a structure dominated by Q^4(4Al) and Q^4(3Al) sites. This shows that the Al content of the K-A-S-H gel is increasing over time, agreeing with the Si/Al ratios shown in Table S4, Supporting Information. Previous work using zeta potential measurements of dispersions of metakaolin particles in solutions representative of the aqueous phase in the fresh geopolymers studied in this work suggest that the dissolution of the metakaolin is slowed due to the adsorption of Sr^{2+} cations to its surface [18]. The results here show that this leads to a Si-rich K-A-S-H gel in the early stages of the reaction (due to the presence of excess soluble silica from the activating solution) which becomes more Al-rich as the sample ages. This is consistent with the FTIR and XRD data for these samples, as well as previous observations by isothermal calorimetry [18]. The calculated extent of reaction shows that the metakaolin precursor continues to react between 3 and 28 days curing.

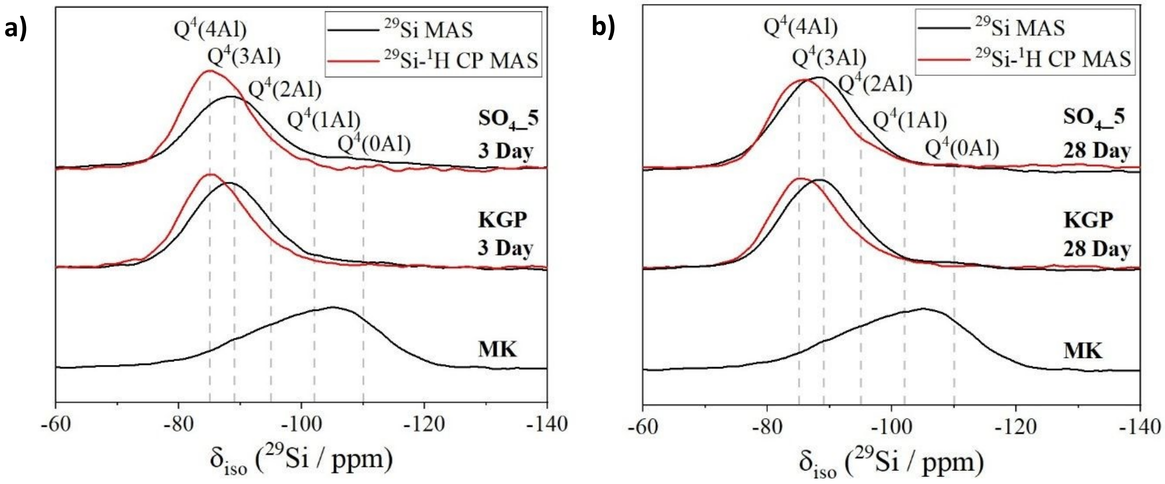

Figure 16: a) ^1H-^{29}Si CP MAS (shown in red, B_0 = 11.7 T, ν_R = 12.5 kHz and Hartmann-Hahn contact period t = 2.0 ms) and b) ^{29}Si MAS (shown in black, B_0 = 11.7 T, ν_R = 12.5 kHz) NMR data and associated deconvolutions for geopolymers cured for 3 and 28d with and without $SrSO_4$, and metakaolin.

3.4.3.2 ^{27}Al and ^{39}K MAS NMR

^{27}Al and ^{39}K MAS NMR data for all samples (Figure 17) are nearly identical to those obtained for geopolymers samples incorporating $Sr(OH)_2.8H_2O$, indicating that Al exists within tetrahedral (q^4) sites in

View Article Online
DOI: 10.1039/D6DT00775A

Open Access Article. Published on 17 June 2026. Downloaded on 6/17/2026 11:56:12 PM.
This article is licensed under a Creative Commons Attribution 3.0 Unported Licence.

the K-A-S-H type gel as well as octahedral Al sites within remnant unreacted metakaolin, and K exists in charge-balancing extra-framework sites within the K-A-S-H-type gel [19, 44]. This is supported by the findings of both the ^{29}Si MAS and ^{1}H-^{29}Si CP MAS NMR data for these samples. No differences in either resonance are observed when comparing samples with and without Sr.

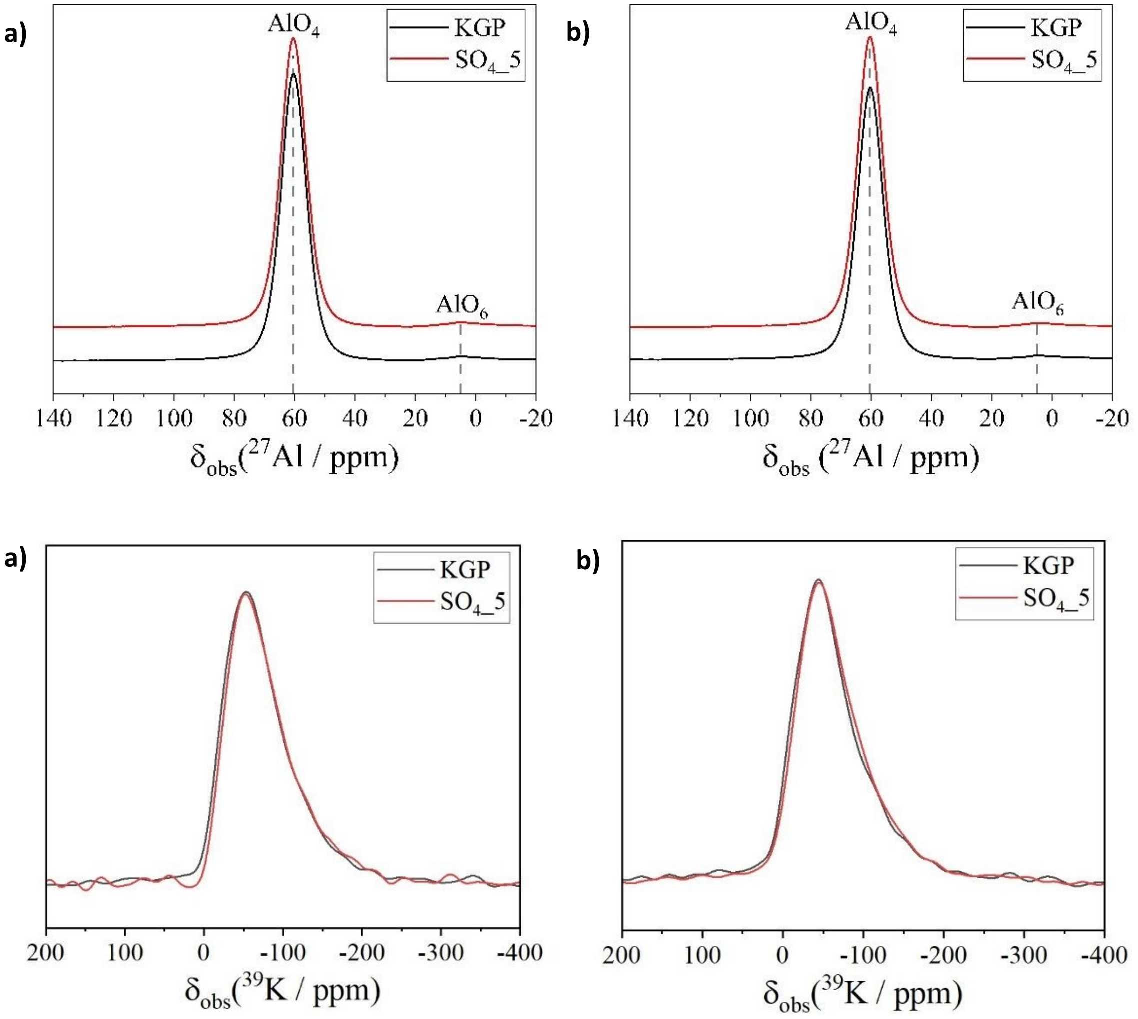

Figure 17: a) ^{27}Al (B_0 = 11.7 T, ν_R = 12.5 kHz) and b) ^{39}K MAS NMR data (B_0 = 20.0 T, ν_R = 12.5 kHz) for each geopolymer cured for 3 and 28 days with and without $SrSO_4$.

The ^{87}Sr NMR data for the SO$_4$_5 sample after curing for 3 and 28 days are shown in Figure 18. As with the data for geopolymers incorporating $Sr(OH)_2{\cdot}8H_2O$ and $Sr(NO_3)_2$, the ^{87}Sr MAS NMR data for the SO$_4$_5 sample after curing for 3 and 28 days exhibits a single distinct resonance with a broad quadrupolar lineshape, centred at approximately δ_{obs} = -33 ppm. This is broadly consistent with the chemical shift and

Dalton Transactions Accepted Manuscript

View Article Online
DOI: 10.1039/D6DT00775A

Open Access Article. Published on 17 June 2026. Downloaded on 6/17/2026 11:56:12 PM.
This article is licensed under a Creative Commons Attribution 3.0 Unported Licence.

Dalton Transactions Accepted Manuscript

FWHM observed for ^{87}Sr MAS NMR data for $SrSO_4$ [61], suggesting that this phase may be responsible for the resonance observed in the data here. The ^{87}Sr MAS NMR data shown in Figure 13 exhibit significant intensity at δ_{obs} = 0 ppm, as a shoulder on the main resonance, consistent with that of the $SrSiO_3$ phase observed in nuclear waste glasses [54]. However, similar to observations for the OH_5 and NO_3_5 samples, this shoulder on the data shown here for the SO_4_5 sample is not significantly above the spectral noise, and so no firm conclusions can be drawn from this data about the existence of this site.

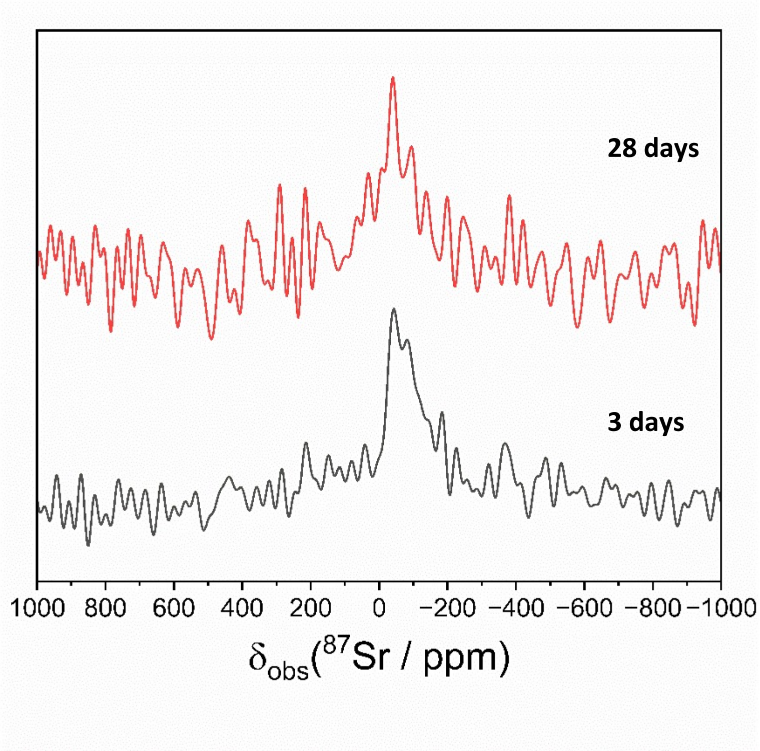

Figure 18: ^{87}Sr MAS NMR data (B_0 = 20.0 T, ν_R = 12.5 kHz with 1024 data points transformed (out of 8192 data points obtained) and line broadening of 100 Hz applied) for the SO_4_5 geopolymer sample cured for 3 and 28 days.

3.4.4 X-ray absorption near-edge structure (XANES) spectroscopy

The normalised spectra for the Sr K-edge XAS analysis of the SO_4_5 sample after both 3 and 28 days of reaction compared to both the $SrSO_4$ reagent and brewsterite-Sr ($(Sr,Ba)_2Al_4Si_{12}O_{32}\cdot10H_2O$) are shown in

View Article Online
DOI: 10.1039/D6DT00775A

Open Access Article. Published on 17 June 2026. Downloaded on 6/17/2026 11:56:12 PM.
This article is licensed under a Creative Commons Attribution 3.0 Unported Licence.

Dalton Transactions Accepted Manuscript

Figure 19 [53]. The Sr K-edge here displays an absorption edge that rises smoothly to a maximum featuring a singular peak. When initially focusing on the peak maximum in Figure 19a), labelled as A, the value of the peak appears to move to slightly higher energies when the $SrSO_4$ is included in the geopolymer mix when compared to the $SrSO_4$ reagent. The energy at which the brewsterite-Sr mineral reaches its maximum peak is comparable to the SO_4_5 samples. This peak can be explored in more detail in Figure 19b), which displays the 1st derivative of this peak. This allows us to further distinguish the features of the leading edge, and shows that there is a potential feature here, most notably in the brewsterite standard. However, the line shape of the spectra for the SO_4_5 samples both follow that of the $SrSO_4$ more closely, with the doublet being far closer to the tip of the peak in both samples.

When exploring the regions above the absorption edge, inspection of the region labelled B in Figure 19a) does not provide a great deal of insight due to the similarities presented here between the $SrSO_4$ standard and the brewsterite standard. However, region C shows that the SO_4_5 samples at both time points relate more closely to the $SrSO_4$ standard than the brewsterite. The spectra here suggest that the Sr within the SO_4_5 samples are likely to exist primarily in $SrSO_4$, as well as incorporated into the K-A-S-H gel as charge balancing cations within a brewsterite-type structure.

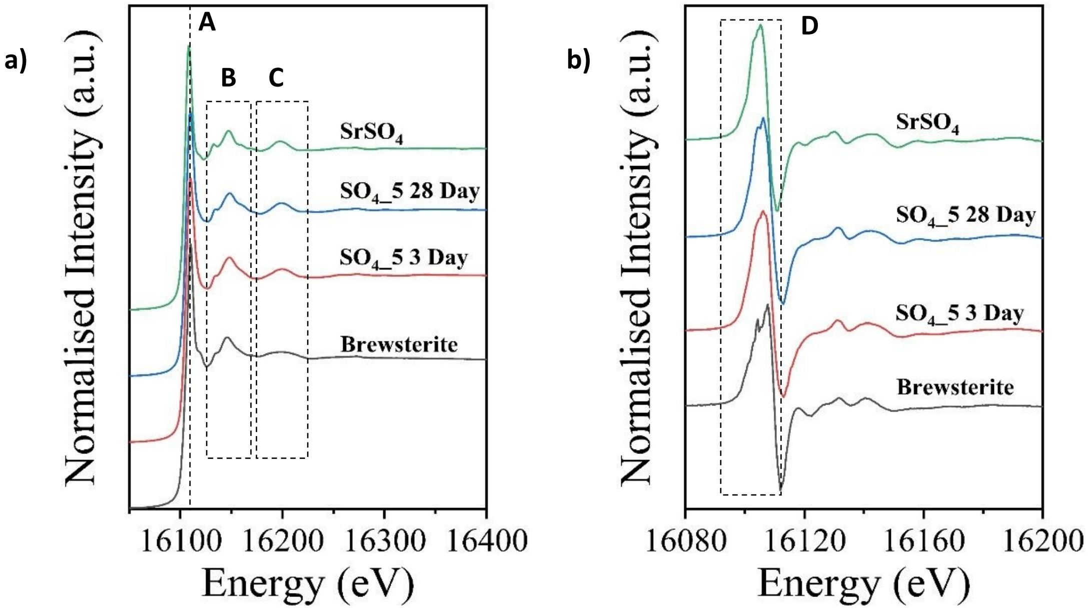

View Article Online
DOI: 10.1039/D6DT00775A

Open Access Article. Published on 17 June 2026. Downloaded on 6/17/2026 11:56:12 PM.
This article is licensed under a Creative Commons Attribution 3.0 Unported Licence.

Figure 19: a) Normalised X-ray absorption spectra for the geopolymer samples loaded with $SrSO_4$, reagent grade $SrSO_4$, and the mineral brewsterite-Sr, and b) the 1st derivative of these spectra.

3.4.5 Electron probe microanalysis

EPMA images of the SO_4_5 sample cured for 28 days are shown in Figure 20, and the data exhibit a distribution of Al, Si, and K consistent with the amorphous K-A-S-H gel framework, with unreacted metakaolin particles (observed as Al-rich regions), similar to the data for geopolymers incorporating $Sr(OH)_2{\cdot}8H_2O$, $SrCO_3$, and $Sr(NO_3)_2$. Sr is present within the sample in multiple phases. Firstly, the regions of very high Sr content, depicted by the red regions in the image, suggest the presence of unreacted and undissolved $SrSO_4$ salt which was added as the reagent. It is likely that this phase is $SrSO_4$ due to the low concentration of the other elements in these areas. This phase is seen throughout the sample, and suggests that the $SrSO_4$ mixed within the geopolymer gel, but has become encapsulated within the gel as opposed to becoming incorporated chemically into the structure in place of the K^+ cations as the charge balancing ion. To add to this, the widespread concentration of K shown in image e) suggests that it is acting as the charge balancing cation in the K-A-S-H gel in the majority of cases. An additional phase is observed that contains relatively high concentrations of both Sr and K (indicated by the white boxes in both images). This phase is potentially that of the kalistrontite that is seen in the XRD analysis, and this is supported by the small concentration of Si that can be seen in these regions. This finding provides further evidence for the reaction between the $SrSO_4$ salt and the activating solution, the only reagent containing K, which is likely to be causing the changes in reaction kinetics observed previously [18].

Dalton Transactions Accepted Manuscript

View Article Online
DOI: 10.1039/D6DT00775A

Open Access Article. Published on 17 June 2026. Downloaded on 6/17/2026 11:56:12 PM.
This article is licensed under a Creative Commons Attribution 3.0 Unported Licence.

Dalton Transactions Accepted Manuscript

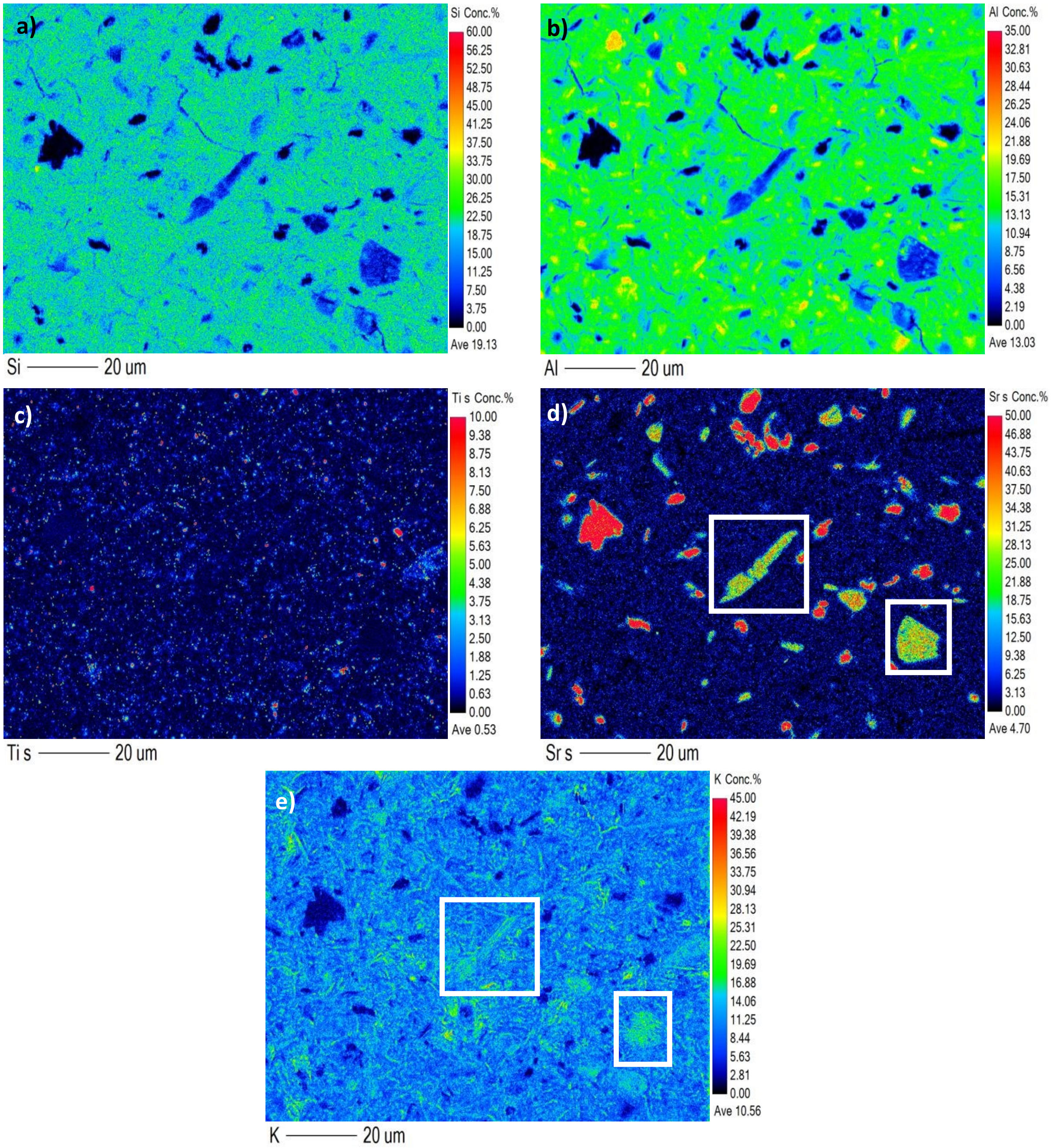

Figure 20: a) Electron probe microanalysis images generated for the SO_4_5 geopolymer cured for 28 days showing distribution of a) aluminium, b) silicon, c) titanium, d) strontium, and e) potassium within the sample.

View Article Online
DOI: 10.1039/D6DT00775A

Open Access Article. Published on 17 June 2026. Downloaded on 6/17/2026 11:56:12 PM.
This article is licensed under a Creative Commons Attribution 3.0 Unported Licence.

4 Conclusions

This study provides a comprehensive analysis of the impact of Sr salt chemistry on the development, mechanisms of reaction, and nanostructural development during K-A-S-H gel formation, of potassium silicate-activated geopolymers. Across all samples, the primary binding phase is a structurally disordered, highly cross-linked K-A-S-H gel. The gel consists of a fully polymerised aluminosilicate framework where Al exists in tetrahedral coordination and Si is distributed across various $Q^4(m\mathrm{Al})$ environments.

The mechanism of Sr incorporation is highly dependent on the solubility of the initial salt. Soluble salts (strontium nitrate and strontium hydroxide) release Sr^{2+} ions that can be chemically incorporated into the geopolymer framework as charge-balancing cations, forming pseudo-zeolitic (brewsterite-type) local structures. Less soluble salts (carbonate and sulfate) remain largely unreacted and become physically encapsulated within the geopolymer matrix. The presence of $Sr(NO_3)_2$ and $SrSO_4$ can alter the early-stage formation of the K-A-S-H gel by delaying metakaolin dissolution by forming a physical or electrostatic shielding layer on the precursor surface, leading to an initially Si-rich gel that becomes increasingly Al-rich as reaction progresses.

In specific cases, chemical reactions between the Sr salts and the alkaline activator lead to new crystalline phases, such as kalistrontite ($K_2Sr(SO_4)_2$) in sulfate-bearing samples or niter (KNO_3) in nitrate-bearing samples. The ability of K-A-S-H geopolymers to accommodate Sr through both chemical substitution in the gel framework and physical encapsulation of discrete salt particles highlights their potential as robust materials for the long-term immobilisation of ^{90}Sr-bearing radioactive waste streams.

Dalton Transactions Accepted Manuscript

View Article Online
DOI: 10.1039/D6DT00775A

5 Acknowledgements

This work has been funded by the Engineering and Physical Sciences Research Council (EPSRC), UK, through grants EP/Y029208/1, and a PhD studentship awarded to Kyle O'Donoghue by the School of Chemical, Materials, and Biological Engineering. The UK 850 MHz solid state NMR Facility used in this work was funded by EPSRC and BBSRC (grant EP/T015063/1), as well as the University of Warwick, including via part funding through Birmingham Science City Advanced Materials Projects 1 and 2 supported by Advantage West Midlands (AWM), and the European Regional Development Fund (ERDF). We acknowledge Diamond Light Source for time on Beamline B18 under Proposal SP37458-1, and thank Dr Diego Gianolio, Principal Beamline Scientist, B18, Diamond Light Source, and Dr Thokozile Kathyola, Senior Support Scientist, for assistance with acquiring the XAS data. We also thank Dr Khalid Doudin, School of Maths, Chemistry, and Physics, The University of Sheffield, for assistance in acquiring some of the NMR data obtained at The University of Sheffield, and Dr Stuart Creasey-Gray, School of Chemical, Materials, and Biological Engineering, The University of Sheffield, for assistance in acquiring the EPMA data.

Open Access Article. Published on 17 June 2026. Downloaded on 6/17/2026 11:56:12 PM.
This article is licensed under a Creative Commons Attribution 3.0 Unported Licence.

Dalton Transactions Accepted Manuscript

View Article Online
DOI: 10.1039/D6DT00775A

Open Access Article. Published on 17 June 2026. Downloaded on 6/17/2026 11:56:12 PM.
This article is licensed under a Creative Commons Attribution 3.0 Unported Licence.

Dalton Transactions Accepted Manuscript

References

1. Marsh, A.I., L.G. Williams, and J.A. Lawrence, *The important role and performance of engineered barriers in a UK geological disposal facility for higher activity radioactive waste.* Progress in Nuclear Energy, 2021. **137**: p. 103736.
2. Bar-Nes, G., et al., *Cesium and Strontium Immobilization in Portland Cement Pastes Blended With Pozzolanic Additives.* Journal of Nuclear Engineering and Radiation Science, 2017. **3**(3).
3. Ojovan, M.I., W.E. Lee, and S.N. Kalmykov, *An introduction to nuclear waste immobilisation*. 2019: Elsevier.
4. Dezerald, L., et al., *Cement as a waste form for nuclear fission products: the case of 90Sr and its daughters.* Environmental Science & Technology, 2015. **49**(22): p. 13676-13683.
5. Tits, J., et al., *Strontium binding by calcium silicate hydrates.* Journal of Colloid and Interface Science, 2006. **300**(1): p. 78-87.
6. Radioactive Waste Management, *Geological disposal: waste package evolution status report*. 2016, RWM-NDA: Didcot, UK.
7. Lehne, J. and F. Preston, *Making concrete change: Innovation in low-carbon cement and concrete.* 2018.
8. Nuclear Decommissioning Authority, Radioactive Waste Management, and Sellafield Limited, *Case study - Forward planning to ensure cement supplies.* . 2019.
9. Walkley, B. and J.L. Provis, *Solid-state nuclear magnetic resonance spectroscopy of cements.* Materials Today Advances, 2019. **1**: p. 100007.
10. Hong, S.-Y. and F. Glasser, *Alkali binding in cement pastes: Part I. The CSH phase.* Cement and Concrete Research, 1999. **29**(12): p. 1893-1903.
11. Kim, B., et al., *Assessment of structural stability and leaching characteristics of phosphate-based geopolymer waste form containing radioactive spent ion exchange resins.* Journal of Nuclear Materials, 2025. **607**: p. 155671.
12. Provis, J.L. and S.A. Bernal, *Geopolymers and related alkali-activated materials.* Annual Review of Materials Research, 2014. **44**: p. 299-327.
13. Provis, J.L., G.C. Lukey, and J.S. van Deventer, *Do geopolymers actually contain nanocrystalline zeolites? A reexamination of existing results.* Chemistry of materials, 2005. **17**(12): p. 3075-3085.
14. Provis, J., *Geopolymers and other alkali activated materials: why, how, and what?* Materials and Structures, 2014. **47**(1-2): p. 11-25.
15. Geddes, D., et al. *Metakaolin-based geopolymers for nuclear waste encapsulation*. in *Calcined Clays for Sustainable Concrete: Proceedings of the 2nd International Conference on Calcined Clays for Sustainable Concrete*. 2018. Springer.
16. Gasperi, J.d., et al., *Effect of Activator Type and Concentration, Water-to-Solid Ratio, and Time on the Flowability of Metakaolin-Based Geopolymer Pastes.* Journal of Materials in Civil Engineering, 2022. **34**(9): p. 04022205.
17. Vance, K., et al., *Observations on the rheological response of alkali activated fly ash suspensions: the role of activator type and concentration.* Rheologica Acta, 2014. **53**: p. 843-855.
18. O'Donoghue, K.T., et al., *Reaction mechanisms and kinetics in geopolymers incorporating strontium salts.* Dalton Transactions, 2025. **54**(29): p. 11337-11348.
19. Duxson, P., et al., *Effect of alkali cations on aluminum incorporation in geopolymeric gels.* Industrial & Engineering Chemistry Research, 2005. **44**(4): p. 832-839.
20. Duxson, P., et al., *29Si NMR Study of Structural Ordering in Aluminosilicate Geopolymer Gels.* Langmuir, 2005. **21**(7): p. 3028-3036.
21. Palomo, A., S. Alonso, and A. Fernández-Jiménez, *Alkaline activation of fly ashes: NMR study of the reaction products.* Journal of the American Ceramic Society, 2004. **87**(6): p. 1141-1145.

View Article Online
DOI: 10.1039/D6DT00775A

Open Access Article. Published on 17 June 2026. Downloaded on 6/17/2026 11:56:12 PM.
This article is licensed under a Creative Commons Attribution 3.0 Unported Licence.

22. Walkley, B., et al., *Incorporation of strontium and calcium in geopolymer gels.* Journal of hazardous materials, 2020. **382**: p. 121015.
23. Walkley, B., et al., *Phase evolution of Na_2O-Al_2O3-SiO_2-H_2O gels in synthetic aluminosilicate binders.* Dalton Transactions, 2016. **45**(13): p. 5521-35.
24. Duxson, P., et al., *^{39}K NMR of free potassium in geopolymers.* Industrial and Engineering Chemistry Research, 2006. **45**: p. 9208-9210.
25. Geddes, D.A., et al., *Alkali-mediated Sr incorporation mechanism and binding capacity of alkali aluminosilicate hydrate in geopolymers.* Journal of Hazardous Materials, 2025. **488**: p. 137426.
26. Bowers, G.M., et al., *NMR study of strontium binding by a micaceous mineral.* The Journal of Physical Chemistry B, 2006. **110**(14): p. 7159-7164.
27. Faucher, A., et al., *Solid-State 87Sr NMR Spectroscopy at Natural Abundance and High Magnetic Field Strength.* The Journal of Physical Chemistry A, 2015. **119**(49): p. 11847-11861.
28. Kye, Y.-S., X. Zhao, and G.S. Harbison, *Orientation of single crystals using linear approximations to NMR transits.* Journal of Magnetic Resonance, 2005. **174**(1): p. 54-59.
29. Moudrakovski, I.L., *Chapter Four - Recent Advances in Solid-State NMR of Alkaline Earth Elements*, in *Annual Reports on NMR Spectroscopy*, G.A. Webb, Editor. 2013, Academic Press. p. 129-240.
30. Provis, J.L., et al., *Statistical Thermodynamic Model for Si/Al Ordering in Amorphous Aluminosilicates.* Chemistry of Materials, 2005. **17**(11): p. 2976-2986.
31. Harris, R.K., et al., *NMR Nomenclature: Nuclear Spin Properties and Conventions for Chemical Shifts: IUPAC Recommendations 2001.* Solid State Nuclear Magnetic Resonance, 2002. **22**(4): p. 458-483.
32. Ravel, B. and M. Newville, *ATHENA, ARTEMIS, HEPHAESTUS: data analysis for X-ray absorption spectroscopy using IFEFFIT.* Journal of synchrotron radiation, 2005. **12**(4): p. 537-541.
33. Lee, W. and J. Van Deventer, *Use of infrared spectroscopy to study geopolymerization of heterogeneous amorphous aluminosilicates.* Langmuir, 2003. **19**(21): p. 8726-8734.
34. Hajimohammadi, A., J.L. Provis, and J.S. van Deventer, *The effect of silica availability on the mechanism of geopolymerisation.* Cement and Concrete Research, 2011. **41**(3): p. 210-216.
35. Farmer, V., *The infrared spectra of minerals: Mineralogical Society.* London, Monograph, 1974. **4**: p. 539.
36. Mozgawa, W., *The relation between structure and vibrational spectra of natural zeolites.* Journal of Molecular Structure, 2001. **596**(1-3): p. 129-137.
37. Alavi, M.A. and A. Morsali, *Syntheses and characterization of $Sr(OH)_2$ and $SrCO_3$ nanostructures by ultrasonic method.* Ultrasonics Sonochemistry, 2010. **17**(1): p. 132-138.
38. Pouhet, R. and M. Cyr, *Studies of natural and accelerated carbonation in metakaolin-based geopolymer.* Advances in Science and Technology, 2014. **92**: p. 38-43.
39. Duxson, P., G.C. Lukey, and J.S.J. van Deventer, *Evolution of Gel Structure during Thermal Processing of Na-Geopolymer Gels.* Langmuir, 2006. **22**(21): p. 8750-8757.
40. Patnaik, P., *Handbook of inorganic chemicals*. Vol. 529. 2003: McGraw-Hill New York.
41. Longhi, M.A., et al., *Metakaolin-based geopolymers: Relation between formulation, physicochemical properties and efflorescence formation.* Composites Part B: Engineering, 2020. **182**: p. 107671.
42. Niu, X., et al., *Incorporation of boron into metakaolin-based geopolymers for radionuclide immobilisation and neutron capture potential.* Cement and Concrete Research, 2025. **190**: p. 107814.
43. Engelhardt, G., et al., *^{29}Si-NMR-Untersuchungen zur Verteilung der Silicium-und Aluminiumatome im Alumosilicatgitter von Zeolithen mit Faujasit-Struktur.* Zeitschrift für anorganische und allgemeine Chemie, 1981. **482**(11): p. 49-64.

Dalton Transactions Accepted Manuscript

View Article Online
DOI: 10.1039/D6DT00775A

Open Access Article. Published on 17 June 2026. Downloaded on 6/17/2026 11:56:12 PM.
This article is licensed under a Creative Commons Attribution 3.0 Unported Licence.

44. Walkley, B., et al., *New structural model of hydrous sodium aluminosilicate gels and the role of charge-balancing extra-framework Al.* Journal of Physical Chemistry C, 2018. **122**(10): p. 5673-5685.
45. Lecomte, I., et al., *(Micro)-structural comparison between geopolymers, alkali-activated slag cement and Portland cement.* Journal of the European Ceramic Society, 2006. **26**(16): p. 3789-3797.
46. Singh, P.S., T. Bastow, and M. Trigg, *Structural studies of geopolymers by 29 Si and 27 Al MAS-NMR.* Journal of materials science, 2005. **40**: p. 3951-3961.
47. Ropp, R.C., *Chapter 3 - Group 16 (O, S, Se, Te) Alkaline Earth Compounds*, in *Encyclopedia of the Alkaline Earth Compounds*, R.C. Ropp, Editor. 2013, Elsevier: Amsterdam. p. 105-197.
48. Smith, H., *The crystal structure of strontium hydroxide octahydrate, Sr (OH) 2.8 H2O.* Acta Crystallographica, 1953. **6**(7): p. 604-609.
49. Reuter, H., S. Kamaha, and O. Zerzouf, *Hydrogen Bonds in the Crystal Structure of Strontium Hydroxide Octahydrate Sr(OH)2 · 8H2O.* 2007. **62**(2): p. 215-219.
50. Arbel Haddad, M., et al., *Formation of zeolites in metakaolin-based geopolymers and their potential application for Cs immobilization.* Journal of Nuclear Materials, 2017. **493**: p. 168-179.
51. Zhang, B., K.J. MacKenzie, and I.W. Brown, *Crystalline phase formation in metakaolinite geopolymers activated with NaOH and sodium silicate.* Journal of materials science, 2009. **44**: p. 4668-4676.
52. Perrotta, A. and J. Smith, *The crystal structure of brewsterite,(Sr, Ba, Ca)(Al2Si6O16). 5H2O.* Acta Crystallographica, 1964. **17**(7): p. 857-862.
53. Artioli, G., J.V. Smith, and Å. Kvick, *Multiple hydrogen positions in the zeolite brewsterite,(Sr0. 95, Ba0. 05) Al2Si6O16. 5H2O.* Acta Crystallographica Section C: Crystal Structure Communications, 1985. **41**(4): p. 492-497.
54. Kroeker, S., *Nuclear waste glasses: insights from solid-state NMR.* NMR of Quadrupolar Nuclei in Solid Materials, 2012: p. 453.
55. Joseph, K., et al., *Iron phosphate glasses: Bulk properties and atomic scale structure.* Journal of Nuclear Materials, 2017. **494**: p. 342-353.
56. Wilke, M., et al., *Oxidation state and coordination of Fe in minerals: An Fe K-XANES spectroscopic study.* American Mineralogist, 2001. **86**(5-6): p. 714-730.
57. Farges, F., et al., *The effect of redox state on the local structural environment of iron in silicate glasses: a combined XAFS spectroscopy, molecular dynamics, and bond valence study.* Journal of Non-Crystalline Solids, 2004. **344**(3): p. 176-188.
58. Lide, D.R., *CRC handbook of chemistry and physics*. Vol. 85. 2004: CRC press.
59. Kemp, S.J., et al., *Kalistrontite, its occurrence, structure, genesis, and significance for the evolution of potash deposits in North Yorkshire, UK.* American Mineralogist: Journal of Earth and Planetary Materials, 2018. **103**(7): p. 1136-1150.
60. Kemp, S., et al., *An improved approach to characterize potash-bearing evaporite deposits, evidenced in North Yorkshire, United Kingdom.* Economic Geology, 2016. **111**(3): p. 719-742.
61. Bowers, G.M., A.S. Lipton, and K.T. Mueller, *High-field QCPMG NMR of strontium nuclei in natural minerals.* Solid State Nuclear Magnetic Resonance, 2006. **29**(1-3): p. 95-103.

Dalton Transactions Accepted Manuscript

All data supporting this article have been included as part of the main manuscript.

View Article Online
DOI: 10.1039/D6DT00775A

Open Access Article. Published on 17 June 2026. Downloaded on 6/17/2026 11:56:12 PM.
This article is licensed under a Creative Commons Attribution 3.0 Unported Licence.

Dalton Transactions Accepted Manuscript